

From Imitation to Refinement – Residual RL for Precise Assembly

Lars Ankile^{1,2,3} Anthony Simeonov^{1,2} Idan Shenfeld^{1,2} Marcel Torne^{1,2} Pulkit Agrawal^{1,2}

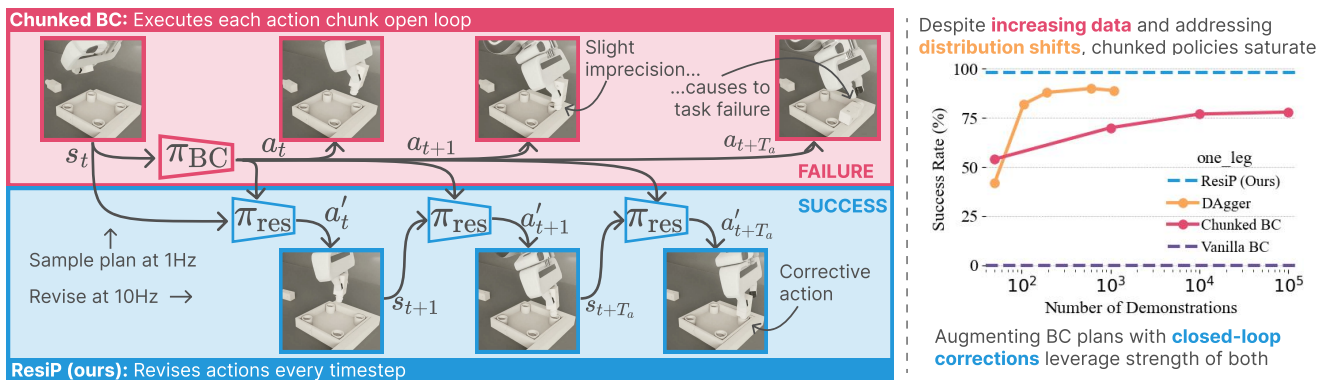


Fig. 1. Left: (Top) Tasks like assembly require long-horizon coordination and high-precision control, at which state-of-the-art BC methods fail due to their chunk-level open-loop nature. **(Bottom)** Combining a BC trajectory planner with a closed-loop residual policy trained with RL results in surprisingly robust and reactive behaviors. **Right: Chunking** improves performance over **standard policy** architectures. Still, performance saturates despite increasing data and addressing distribution shifts with DAgger [1]. Combining chunking with **closed-loop corrections** (ResiP) combines the strength of each.

Abstract—Recent advances in behavior cloning (BC), like action-chunking and diffusion, have led to impressive progress. Still, imitation alone remains insufficient for tasks requiring reliable and precise movements, such as aligning and inserting objects. Our key insight is that chunked BC policies function as trajectory planners, enabling long-horizon tasks. Conversely, as they execute action chunks open-loop, they lack the fine-grained reactivity necessary for reliable execution. Further, we find that the performance of BC policies saturates despite increasing data. Reinforcement learning (RL) is a natural way to overcome this, but it is not straightforward to apply directly to action-chunked models like diffusion policies. We present a simple yet effective method, ResiP (*Residual for Precise Manipulation*), that sidesteps these challenges by augmenting a frozen, chunked BC model with a fully closed-loop residual policy trained with RL. The residual policy is trained via on-policy RL, addressing distribution shifts and introducing reactivity without altering the BC trajectory planner. Evaluation on high-precision manipulation tasks demonstrates strong performance of ResiP over BC methods and direct RL fine-tuning.

Videos, code, and data are available at <https://residual-assembly.github.io>.

I. INTRODUCTION

Robotic manipulation tasks that require both long-horizon planning and high-precision control, such as assembly, remain a significant challenge in robotics [2]–[6]. As an example, consider the furniture assembly task depicted in Fig. 1 (Left), where a robot performs assembly by sequentially grasping and then re-orienting a table leg into the correct pose, performing a precise insertion, and finally screwing the leg in place. This representative task involves executing a specific sequence of skills over hundreds of timesteps, with

each stage dependent on the successful completion of the previous. Small imprecisions anywhere in the chain can lead to task failure, underscoring the need for reliable execution of diverse skills in the sequence.

Behavior cloning (BC) is a popular approach for teaching robots various manipulation skills [6]–[15]. Recent innovations in BC, such as diffusion models [16]–[19] and action chunking [6, 16, 18, 20], have improved learning long-horizon, complex behaviors from demonstrations [15, 21]. However, our analysis shows fundamental limitations in BC when applied to tasks requiring high precision. For example, in the insertion task shown in Fig. 1 (Left), a diffusion-based BC model achieves a success rate of ~50% with a handful of demonstrations, but performance plateaus even when scaling up to large datasets (e.g., 100,000 demonstrations), reaching only about ~80% success, as seen in Fig. 1 (Right). Other recent work finds similar performance saturation [22]–[24].

We hypothesize that this saturation occurs because of two issues: First, BC methods suffer from compounding errors due to distributional shifts; the policy operates on states that deviate from those seen during training, leading to errors that accumulate over time [22]. While approaches like Dataset Aggregation (DAgger) [1] can mitigate this error mode by collecting on-policy data, such approaches assume an expert who can be queried on demand, which is usually unavailable. Second, modern BC policies, particularly ones employing action chunking, act more like open-loop “planners” than reactive controllers. Chunked BC policies are limited in compensating for noise and disturbances (i.e., non-reactive) because each chunk runs in an open loop. In tasks such as furniture assembly, certain “bottleneck” states, like insertions, require precise actions at specific time steps.

¹Improbable AI Lab ²Massachusetts Institute of Technology ³Harvard University ankile@mit.edu

If these critical moments fall within an action chunk, the BC trajectory planner cannot make real-time adjustments to compensate for inaccuracies in the planned actions. This inability to correct actions leads to task failure in high-precision tasks.

Reinforcement Learning (RL) promises to autonomously learn corrective behaviors through interaction and exploration guided by a reward function [25,26]. RL has been effective in training robust reactive controllers that can handle a wide array of tasks [27]–[31]. However, applying RL to solve complex, long-horizon, and precise tasks like robotic assembly requires extensive reward engineering that can be prohibitively difficult and time-consuming [32]. RL requires vast data, which is costly to collect, particularly in real-world settings.

We present a way to leverage the strengths of BC and RL that reduces human effort in obtaining reliable policies by building on recent advances in BC methods and sim-to-real RL training. BC learns a “planner” that predicts trajectory segments (i.e., an action chunk executed open loop) conditioned on the agent’s observations from a small set of demonstrations, providing a skeleton for RL training. RL augments the BC-learned planner with a closed-loop controller capable of fine-grained corrections that mitigate the limitations of open-loop action chunk execution and collects on-policy data to ensure reliable plan execution. While combining BC and RL has a long history [33]–[45], the recent advancements in BC architectures present new challenges for fine-tuning the learned policy with RL. The structure of diffusion models (iterative refinement) and action-chunked policies (large action spaces) complicate the application of standard RL algorithms, often leading to instability or requiring significant architectural modifications [15,46,47].

We propose a simple yet effective method to combine the strengths of modern chunked BC and on-policy RL controllers, called *ResiP* (*Residual for Precise Manipulation*), shown in Fig. 2. Our key insight is recognizing that modern BC policies function as trajectory planners that generate action sequences but crucially lack the fine-grained reactivity and corrections required for reliable execution. We introduce closed-loop corrections by augmenting a frozen, chunked BC model with a small, single-step residual policy trained via on-policy RL. The residual policy observes each state and action and predicts a corrective action to be added to the action predicted by the BC model. This design sidesteps the difficulties of fine-tuning complex BC models with RL while addressing BC’s limitations. First, the residual RL policy operates on-policy, learning reactive behaviors directly through interaction with the environment, thus overcoming issues of distributional shift. Second, providing closed-loop control enables real-time adjustments during task execution, improving robustness and precision, especially in bottleneck stages like insertions. Finally, the residual training is supervised with a sparse task-completion reward, avoiding reward engineering.

We evaluate *ResiP* on a range of high-precision manipulation tasks from the challenging FurnitureBench [5] and

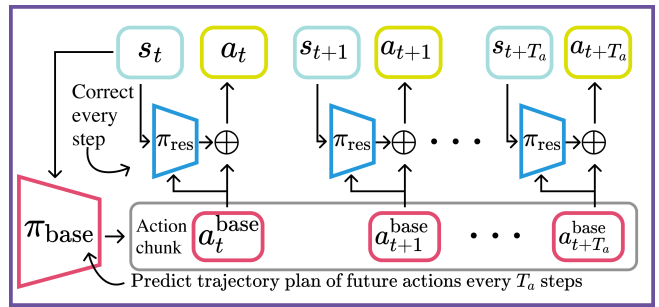


Fig. 2. Overview of *ResiP*. A pretrained **chunked base policy** predicts an action chunk of T_a future actions. For every timestep, the **residual model** observes the current state s_t and predicted base action a_t^{base} and corrects.

Factory [48] benchmarks. Our experiments demonstrate that *ResiP* outperforms pure BC methods and traditional RL fine-tuning, achieving success rates up to $\sim 97\%$ starting from 50 demonstrations. At the same time, increasing data for BC saturates at $\sim 80\%$ success with 100K demonstrations. We also find that *ResiP*, combined with straightforward applications of teacher-student distillation, visual domain randomization, and co-training, we can transfer policies from simulation to physical robot hardware using RGB observations.

II. PROBLEM SETUP AND APPROACH OVERVIEW

a) Assumptions and System Components: Our method applies to tasks that can be simulated using already available assets (e.g., CAD models) or using assets that can be obtained via scans of real-world environments [30]. While our method is general, we empirically verify it on a set of challenging assembly tasks of `one_leg`, `round_table`, and `lamp` taken from the FurnitureBench [5] task suite, the `peg-in-hole` task from [48], a custom mug-hanging task we call `mug-rack`, and a custom bimanual precise insertion task we call `biman-insert`. Visualizations and detailed task descriptions are provided on the [project website](#) and in [Sec. II](#). Multi-part assembly interactions are simulated using the SDF-based collision geometry representations provided as part of the Factory [48] extension of NVIDIA’s Isaac Gym simulator [49]. The `biman-insert` task is implemented using the MuJoCo simulator [50].

We define a sparse task-completion reward set to 1 for each task when a pair of parts has been fully assembled and 0 otherwise. Many of our tasks are long horizon (up to ~ 750 -1000 steps at 10Hz) and require sequencing of behaviors such as 6-Degree-of-Freedom (DoF) grasping, reorientation, insertion, and screwing (see, e.g., [Fig. 1](#) (Left)).

b) Preliminaries: Each task is formulated as a discrete-time sequential decision-making problem. At every time-step t , the robot receives an observation $o_t \in \mathcal{O}$ corresponding to the world/robot state $s_t \in \mathcal{S}$ (available only in simulation) and uses it to predict an action a_t that is then executed.

The policy operates at 10Hz on a 7-DoF Franka Emika Panda robot arm for all tasks but `biman-insert`, which

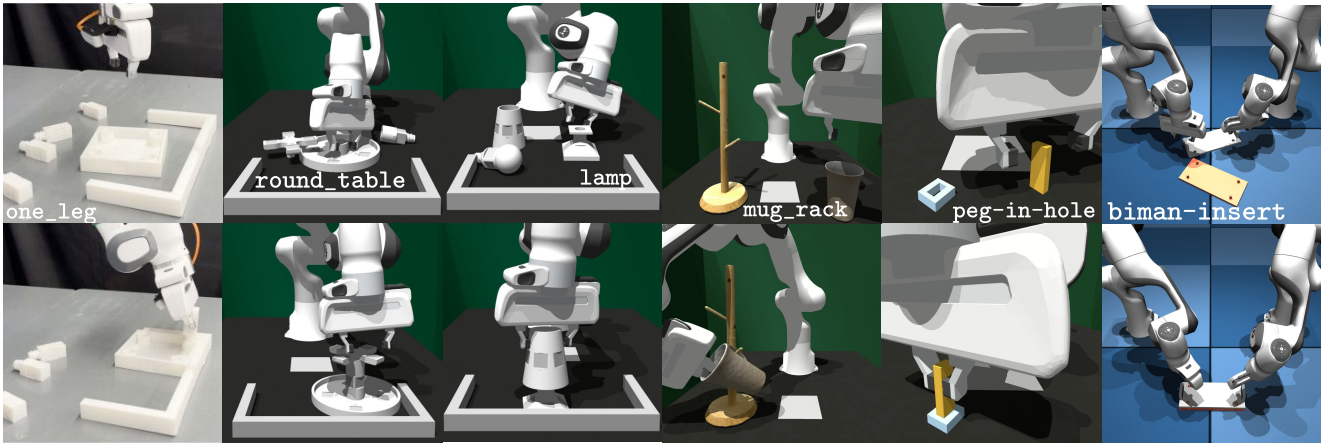


Fig. 3. Initial and goal states for our 6 tasks. The first three tasks, `one_leg`, `round_table`, and `lamp`, come from the FurnitureBench [5] task suite. `mug_rack` we created by scanning objects and importing into the simulation. `peg-in-hole` is from the Factory [48] task suite. `biman-insert` we created using an upcoming simulation-based teleoperation system. Our task suite exhibits diverse challenges like long horizons, tight tolerances, bimanual control, and multi-modal success criteria.

operates at 50Hz on two Franka Panda arms. The action space consists of the desired end-effector pose $\mathbf{T}^{\text{des}} \in \text{SE}(3)$, which includes both position and orientation and a binary gripper command for opening/closing the parallel-jaw gripper. These desired end-effector poses are converted to joint position targets using differential inverse kinematics [51], which are then tracked using a low-level PD controller running at 1KHz with manually specified stiffness and dampening parameters.

In the simulated task variants, the system states space \mathcal{S} contains the same end-effector pose \mathbf{T} , spatial velocity \mathbf{V} , and gripper width w_g , along with the 6-DoF poses of all the parts in the environment $\{\mathbf{T}^{\text{part}_i}\}_{i=1}^{\text{num.parts}}$. In addition to the state/observation, the simulated agent receives a binary reward signal, indicating whether a pair of assembly parts has achieved their required geometric alignment. For example, in the `lamp` task, the policy receives two binary rewards: the first when the bulb is fully screwed in and the second when the lamp shade is successfully placed. The real world observation space \mathcal{O} contains the robot end-effector pose $\mathbf{T} \in \text{SE}(3)$, robot end-effector spatial velocity $\mathbf{V} \in \mathbb{R}^6$, the gripper width w_g , and RGB images from a fixed front-view camera ($I^{\text{front}} \in \mathbb{R}^{h \times w \times 3}$) and a wrist-mounted camera ($I^{\text{wrist}} \in \mathbb{R}^{h \times w \times 3}$), each with unknown camera poses.

III. METHODS

A. Imitation Learning

For each task, we collect a dataset of 50 demonstrations in simulation by teleoperating the robot, $\mathcal{D}_{\text{sim}} : \{\tau_1, \dots, \tau_N\}$ to train a “base” policy that serves as the starting point for RL training. Each trajectory, τ , contains system states s_t , and robot actions a_t , i.e., $\tau_i = \{(s_t, a_1), \dots, (s_T, a_T)\}$, with T being the trajectory length.

\mathcal{D}_{sim} is used to train base policy π_{base} with Behavior Cloning (BC), i.e., $\max_{\pi} \mathbb{E}_{(a_t, s_t) \sim \mathcal{D}_{\text{sim}}} [\log \pi(a_t | s_t)]$. We use a Diffusion Policy [18] as the base model, which has shown

strong empirical performance in handling difficult manipulation tasks with relatively small datasets [21]. Consistent with recent advancements [6,18], our policy framework enhances its performance by predicting multiple future actions in chunks instead of individual actions at each timestep. We denote the length of future action sequences predicted by the policy as T_a , the output as $\mathbf{a}_t = [a_t, \dots, a_{t+T_a}]$. When predicting an action chunk \mathbf{a}_t of length T_a , we only execute a subset $[a_t, \dots, a_{t+T_{\text{exec}}}]$, with execution horizon $T_{\text{exec}} \leq T_a$.

B. Online Reinforcement Learning with Residual Policies

Given the initial base policy π_{base} , we aim to improve it using RL. However, directly fine-tuning diffusion models with RL is an active area of research [46,52]–[54], made difficult because of the multi-step inference process and unavailability of the policy action log-probabilities. Another category of methods upweight high-quality model outputs via importance sampling, return conditioning, or augmenting the original de-noising objective with a loss term for maximizing a Q-function [17,55]–[58]. However, these methods mainly enable better *extraction* of high-quality behavior in the data, while we are more concerned with learning new, *corrective* behaviors. Action chunks can also make optimization with policy gradients more difficult. This is partly due to chunking increasing the effective action space (e.g., chunks of 8 actions increase the dimension $8\times$), which we find to increase RL training instability (see [Sec. IV-A](#)). This means fine-tuning other popular BC architectures, like the Action-Chunked Transformer (ACT) [6], also brings technical challenges [15]. Even with successful RL fine-tuning, the improved policy will still be a trajectory planner lacking in closed-loop reactive control ([Fig. 5](#)). Finally, recent work has shown that fine-tuning large pre-trained models can lead to forgetting of capabilities if the agent does not visit states seen during pre-training frequently enough [59].

We side-step these complications by training a residual

Methods	one_leg		round_table		lamp		mug-rack	peg-in-hole	biman-insert	
	Low	Med	Low	Med	Low	Med	Low	Low	Low	
IL	MLP-S	0	0	0	0	0	0	2	0	
	MLP-C	45	10	5	2	8	1	21	7	
	DP	54	29	12	4	7	2	26	33	
RL	MLP-C + PPO	70	28	38	6	32	2	23	4	30
	DP + IDQL	52	27	18	3	11	1	31	3	40
	ResiP (ours)	98	76	94	77	97	70	88	99	93

TABLE I. Top BC-trained MLPs without chunking (MLP-S) cannot perform any of the tasks, and Diffusion Policies (DP) generally outperform MLPs with chunking (MLP-C). **Bottom** Training our proposed residual policies with RL on top of frozen DP performs the best among the evaluated fine-tuning techniques. The best checkpoint is chosen for all methods, and we average over 1024 rollouts to get the success rate.

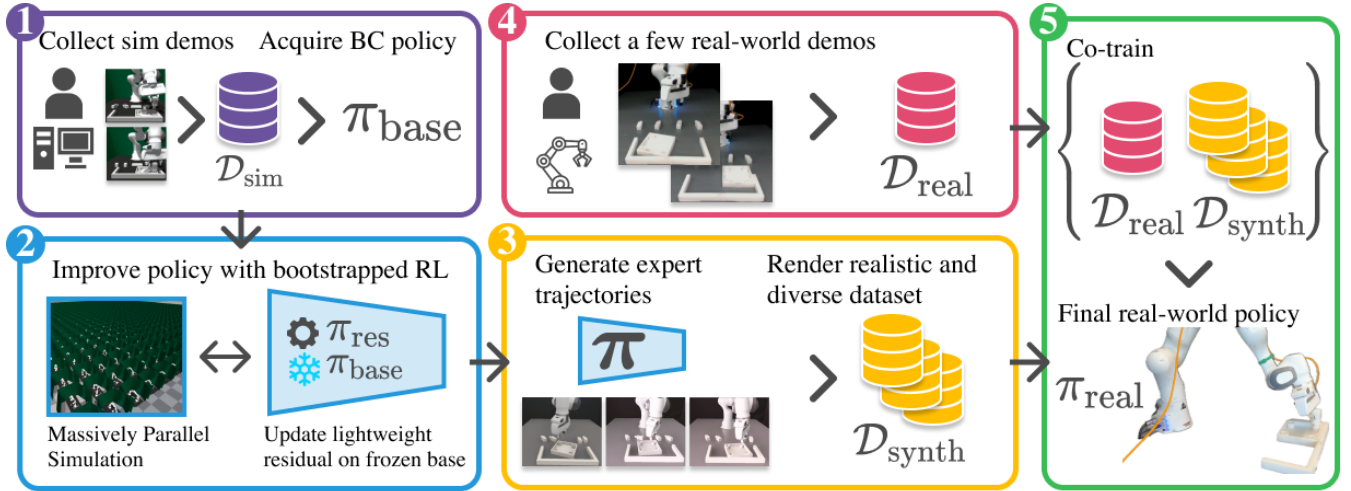


Fig. 4. Sim-to-real pipeline. (1) Beginning with a policy trained with BC in simulation, (2) we train residual policies with RL and sparse rewards. (3) We then distill the resulting behaviors into a policy operating from RGB images. (4) By combining synthetic data with a small set of real demonstrations, (5) we deploy RGB-based policies in the real world.

Gaussian MLP policy π_{res} . This policy takes as input both the system state and the action predicted by the diffusion policy π_{base} and produces an “action correction” that modifies the action as $a_t = a_t^{\text{base}} + \alpha \cdot a_t^{\text{res}}$, with $\alpha \leq 1$ being a coefficient controlling what scale the residual policy operates on. We find that the policy is not sensitive to α in isolation, but rather the resulting exploration noise, $\alpha \mathcal{N}(0, \sigma^{\text{init}} \text{std} I)$. We denote the resulting combined policy π . This decoupling has several advantages. First, we can regard the diffusion model as a black box and not change its parameters [60]. This decoupling also means that ACT (see Sec. IX-B) and other BC methods can serve as the base model without changing the method – an advantage of residual policy learning emphasized by prior robotics work [60,61]. This also allows different prediction horizons T_a for the two policies. This flexibility in action horizon is helpful as most RL algorithms optimize single-action policies and allow the residual to be fully closed-loop. It also removes the need to explicitly regularize the fine-tuned policy to stay near the pre-trained policy, which is often necessary to achieve stable optimization [62,63].

Given the above, we train the π_{res} using standard PPO [26] with the alternation that we augment the state space with the base action. The base model observes the current state s_t and outputs a chunk of actions \mathbf{a}_t . For each action in the chunk, we concatenate it with the current observation $s_{t+i}^{\text{res}} = [s_{t+i}, a_{t+i}^{\text{base}}]$, and predict the correction $a_{t+i}^{\text{res}} \sim \pi^{\text{res}}(\cdot | s_{t+i}^{\text{res}})$ for $i = 0, \dots, T_a - 1$. Besides the technical convenience, one can look at residual policy as a way to incorporate an inductive bias that the policy should mostly learn *locally* corrective actions [61]. This is motivated by our qualitative observations that most of the base BC policy failures are due to slight imprecision near “bottleneck” transitions when performing skills like grasping and insertion (e.g., Fig. 1 (Left)).

C. Sim-to-real pipeline

Ultimately, we are interested in what capabilities our method can enable on real robots. To that end, we devise a sim-to-real pipeline to transfer state-based policies trained in simulation to RGB-based policies deployable on physical hardware. We present the general pipeline in Fig. 4. Once the RL training has converged, the combined pol-

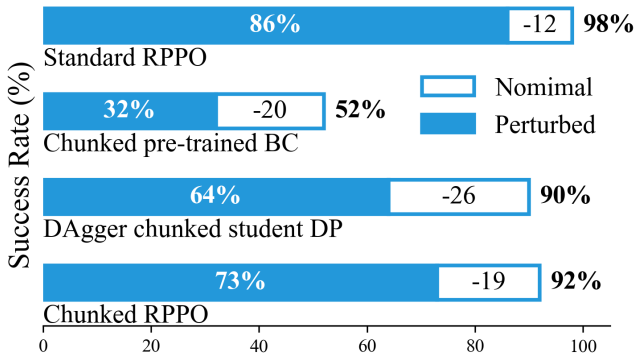


Fig. 5. Perturbations highlight `ResIP`'s resilience: 12% drop vs. 19-26% for chunked methods. See [Sec. IX-A](#) for more detailed discussion.

icy has attained closed-loop correction behavior. We aim to distill this enhanced performance from the state-based policy into a vision-based policy that operates from RGB images. Following the established teacher-student distillation paradigm [31,64,65], we generate a dataset of successful trajectories, $\mathcal{D}_{\text{synth}}$, where the environment's observations, o_t , replace the states, i.e., $\mathcal{D}_{\text{synth}} = \{\tau_{\text{synth},1}, \dots, \tau_{\text{synth},N}\}$ and $\tau_{\text{synth},i} = \{(o_1, a_1), \dots, (o_T, a_T)\}$. For real-world transfer, we enhance the synthetic dataset $\mathcal{D}_{\text{synth}}$ by re-rendering its trajectories in Isaac Sim [66]. This process improves image quality and introduces variability in environmental conditions such as object and table colors, textures, lighting, and camera perspectives, many of which cannot easily be done with standard image augmentation techniques. We denote this refined dataset as $\mathcal{D}_{\text{synth-render}}$. To ease the difficulty of zero-shot sim-to-real with RGB images, we opt for a co-training approach, integrating the synthetic dataset with a small set of real-world task demonstrations, $\mathcal{D}_{\text{real}}$, which similarly comprises only environmental observations without ground truth poses. This combined dataset, $\mathcal{D}_{\text{real}} \cup \mathcal{D}_{\text{synth-render}}$, is used to train the final student policy with BC.

IV. EXPERIMENTS AND RESULTS

In [Sec. IV-A](#), we investigate the requirement of complex BC methods and the impact of our residual reinforcement learning approach on improving the success rates of policies trained with imitation learning. Next, in [Sec. IV-B](#), we study the performance of downstream distillation from synthetic RL data, examining the relationship between the quantity and quality of the data and the resulting performance of the distilled vision-based policies. Finally, in [Sec. IV-C](#), we apply our approach to real robot hardware, enabling precise assembly tasks on a physical robot directly from vision.

A. Improving Imitation Learning with Residual Learning

a) Why Action Chunking and Diffusion Policies?:

Simple feed-forward MLPs of modest size have shown impressive performance in many domains when trained with RL [30,64,65], and offer a natural starting point for RL fine-tuning after BC pre-training. However, MLP policies trained

to directly output single action control instead of a trajectory plan through an action chunk (MLP-S) fail across all tasks we consider. Therefore, we also trained MLP policies with action chunking (MLP-C). When we introduce chunking, MLP performance improves drastically, as shown in [Tab. I](#). However, we also find that the more complex Diffusion Policy (DP) architecture generally outperforms MLPs, especially in tasks of intermediate difficulty. For example, an improvement from 10% success rate to 26% for the `one_leg` task on medium randomness made subsequent fine-tuning far easier.

In one case, `lamp` on low randomness, MLP-C outperformed DP. In qualitative evaluations, we find that DP has smoother and faster actions, which is generally beneficial. Still, it seems to hurt performance in this case, as it tends to retract before the gripper closes. We also find that all methods struggle with the most challenging tasks, on which MLP-C and DP both achieve less than 5% success rate, indicating that there is still room for improvement in BC methods. The `peg-in-hole` task, despite its relatively short horizon of ~ 100 timesteps, proved particularly challenging for BC methods. This task involves a ~ 0.2 mm clearance insertion, resulting in a 5% success rate. This poor performance on a short yet precise task lends credence to the hypothesis that BC methods are ill-equipped to handle high-precision requirements.

Another interesting finding is that the DP is significantly more robust to noise, an important property for an adequate base policy for residual fine-tuning. In contrast, we observed performance collapse when using MLP-C as the base, further reinforcing the utility of using powerful generative models for BC pre-training. See more analysis in [Sec. IX-B](#).

b) *Online Policy Fine-Tuning Comparison:* Next, we investigate the effectiveness of our residual RL approach, `ResIP`, in improving the performance of policies trained with BC. We train residual policies using PPO [26] on top of the diffusion policy and compare it to two baselines – (1) directly fine-tune the MLP-C with PPO while regarding every action chunk as one concatenated action and (2) a chunked version of the IDQL algorithm [55]. In the IDQL algorithm, multiple action samples are retrieved from the diffusion policy, and one chooses the action chunk to execute based on its Q-value. We have found that learning a good Q-value estimator from offline data alone, as proposed in IDQL, is challenging with only 50 demonstrations. Therefore, we learn it in on-policy matter similar to [67].

The results in [Tab. I](#) show that our residual RL approach significantly improves success rates over BC and outperforms alternative RL fine-tuning methods. For tasks with lower initial randomization, such as the `one_leg` task, the residual policy increases the success rate from 54% to 98%. Even more drastically, for the `peg-in-hole` task, `ResIP` improved the success rate from 5% to 99%. However, we observe performance saturates at lower success rates (e.g., $\sim 70\%$) for tasks with higher part randomization. We hypothesize that the base model's performance limits the residual policy as it is designed to act locally, constrained by the base.

Training data	Corner		Grasp		Insert		Screw		Complete	
	Part	Obs	Part	Obs	Part	Obs	Part	Obs	Part	Obs
10 Real	5/10	5/10	5/10	7/10	2/10	3/10	0/10	2/10	0/10	2/10
10 Real + 350 Sim	9/10	9/10	7/10	8/10	0/10	3/10	0/10	3/10	0/10	3/10
40 Real	10/10	8/10	9/10	8/10	6/10	3/10	2/10	3/10	2/10	3/10
40 Real + 350 Sim	10/10	10/10	9/10	10/10	6/10	7/10	5/10	6/10	5/10	6/10

TABLE II. We investigate the effect of combining real-world demonstrations with simulation trajectories from our RL-trained residual policies. Co-training with real and synthetic data improves motion quality and success rate on the `one_leg` task.

Fig. 1 (Left) qualitatively shows the most common failure mode of the BC policies and how the RL policy overcomes it. For instance, a typical BC policy error is to push down before the leg is aligned with the hole. This often results in a shift of the object in the grasp, which causes the policy to diverge due to the out-of-distribution grasp pose. The residual policy reliably corrects these errors by performing small sideways translations while canceling premature downward motions. It typically only allows the leg to be inserted once it is properly above the hole. We also find the residual policy is better at performing initial grasps that allow accurate downstream alignment between the grasped object and the receptacle. On the other hand, the BC policies more often grasp the object at angles that make insertion more difficult. In Fig. 6, we qualitatively analyze this and find that the residual makes the precise insertion part of the task significantly more reliable.

Surprisingly, the residual RL procedure also leads to the emergence of qualitatively different behaviors. We refer to the [website](#)’s uncut videos of rollouts for the pre-trained and fine-tuned policies. In these videos, we observe that the fine-tuned policy has learned new grasps of the table foot that were not demonstrated, as well as more persistent retrying behavior and recovery.

In addition to improved success rates, we observed different training dynamics across each method. First, direct MLP-C fine-tuning proved unstable and required KL-regularization to avoid collapse. Second, the trained DP produced actions with low variance, even with $\eta = 1$ in the DDIM sampler [68], inhibiting Q-learning and constraining the potential for policy improvement. Finally, residual policy training was very stable, likely because it is constrained to operate on a local scale, which prevents large deviations that can make RL unstable and has a small parameter count compared to the base policy [69,70].

c) What drives residual RL performance?: To further understand what drives the residual RL fine-tuning approach’s performance, we try to decompose it into an on-policy component and a fully closed-loop, reactive component.

The impact of on-policy learning is probed by comparing learning the task by scaling the purely offline data versus learning online with DAgger [71]. The performance impli-

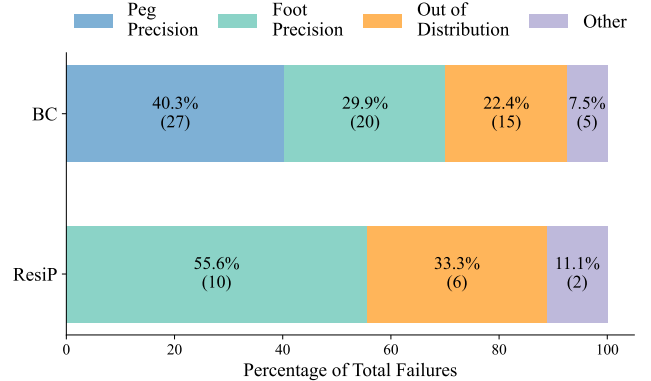


Fig. 6. A qualitative analysis of the failure modes between the pre-trained BC policy and the fine-tuned residual policy for the `round_table` task on medium randomness. For the pre-trained policy, a large portion of the failures (40%) relates to the table leg’s insertion precision. In the fine-tuned policy, this share dropped to 0%.

cations of distillation are further addressed in Sec. IV-B. We find that when applying DAgger for the same action-chunked diffusion policy, we can improve performance significantly over the purely offline case, as shown in Fig. 1 (right) and Fig. 7. However, a gap remains between the residual RL and DAgger policy of 9% and 23% for the `one_leg` and `round_table` tasks, respectively.

On the other hand, we also find the residual policy’s closed-loop, single-step nature helpful. First, when trying to learn a residual policy for whole chunks, the resulting policy learns significantly more slowly, and the performance saturates at a lower level than that of the full closed-loop policy. See Sec. IX-A for details. Furthermore, as shown in Fig. 5, the effect of fully closed-loop control becomes clear when we introduce randomly sampled force perturbations to the episode rollouts. Performance for the ResiP policy drops 12 percentage points, compared to 19-26 percentage points for alternative chunked methods (BC, DAgger, chunked residual).

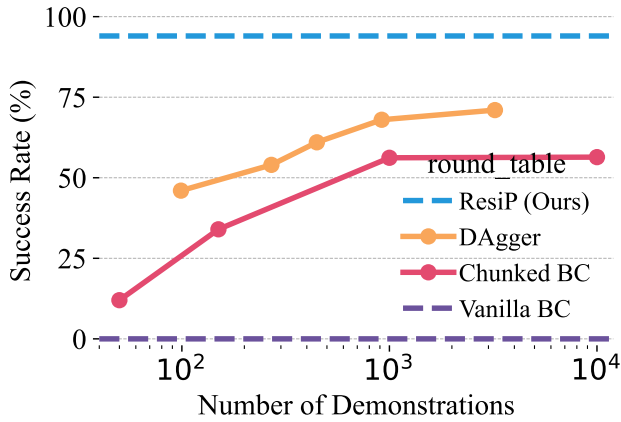


Fig. 7. When scaling up the offline dataset for the harder `roundtable` task, the same trends emerge as for `one_leg` (seen in Fig. 1 (right)), but with saturation happening at a lower success rate of 56%. Again, correcting for distribution shifts with DAGger improves performance but saturates at 71%.

B. Distillation Performance from Synthetic RL Data

Next, we study how synthetic RL data quantity and quality impact the performance of distilled vision-based policies. First, we find that distilling trajectories from the RL agent performs better than training directly on the 50 demonstrations. A vision-based policy distilled from the RL-trained teacher reached 73% on `one_leg`, outperforming the 50% achieved by training the vision policy directly on human demos, see Fig. 8. However, we also observe a performance gap between the RL-trained teacher (98%) and distilled vision-based student policy (73%). We consider whether this gap may be caused by training the student to operate on images. Upon examination, we find that distilling the same number of teacher rollouts into an image-based student and a state-based student results in comparable performance. This leads us to conclude that the change in modality is not the primary source of the performance gap.

Therefore, we also examine the impact of the distillation dataset size. Here, we scale up the number of state-based rollouts from the trained RL policy and distill these to a state-based student. In Fig. 1 (Right), we see that performance increases with more data but still does not reach the performance achieved by the teacher policy, with a gap of 20 percentage points between the best student policy (78% success rate) and the teacher policy (98% success rate) at 100k trajectories (with only a minor improvement from 77% at 10k trajectories). The same trend is evident in Fig. 7. Nevertheless, the improved performance obtained by training with more data highlights the advantage of using simulation for obtaining large-scale synthetic datasets.

DAGger [1] demonstrates significantly greater sample and computational efficiency than pure BC. As shown in Fig. 1 (right), DAGger achieves superior performance to BC trained on 50 human demos in just ~ 10 k gradient steps (with 800

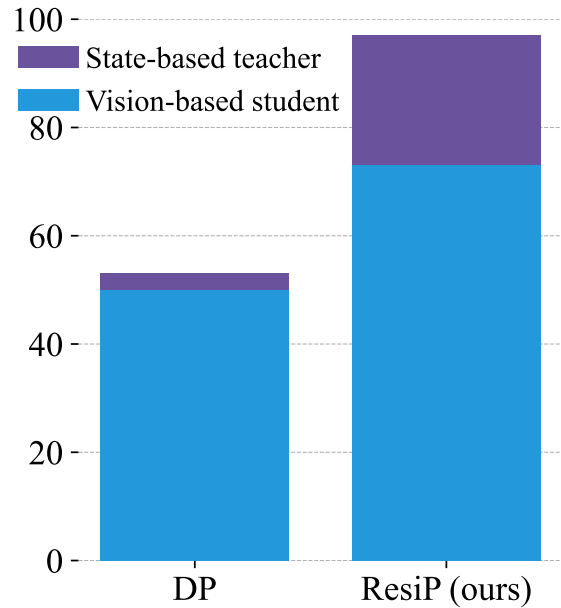


Fig. 8. Comparison of distilled performance from BC and RL-based teacher. On the left, BC policies trained on the same set of demonstrations achieve comparable performance for state and image observations. On the right, the vision-based student policy has a similar performance gap to the state-based teacher as for state-to-state distillation.

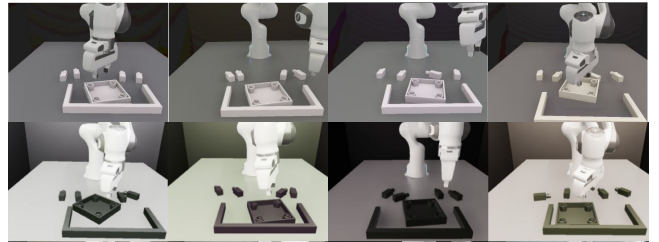


Fig. 9. Examples of photo-realistic rendering and domain randomization for sim-to-real transfer. In the first row, we show our nominal experiment setting of rendering parts in the original white color while varying the position, brightness, and hue of the lighting in the scene. In the bottom row, we also introduce variations in the part colors to see how that can help the final policy adapt to unseen part appearances without collecting any additional data.

rollouts) and surpasses our best BC distillation results at ~ 20 k steps (with ~ 1.5 k demonstrations). These results underscore the advantages of interactive learning over passive offline learning and point towards effective online distillation techniques to help close the gap between the state-based RL-trained experts and the distilled real-world policies deployed on real hardware (see Sec. IV-C).

C. Real-World Application

Finally, we evaluate the real-world performance of a sim-to-real policy trained on a mixture of a few (10/40) real-world demonstrations and simulation data generated by the

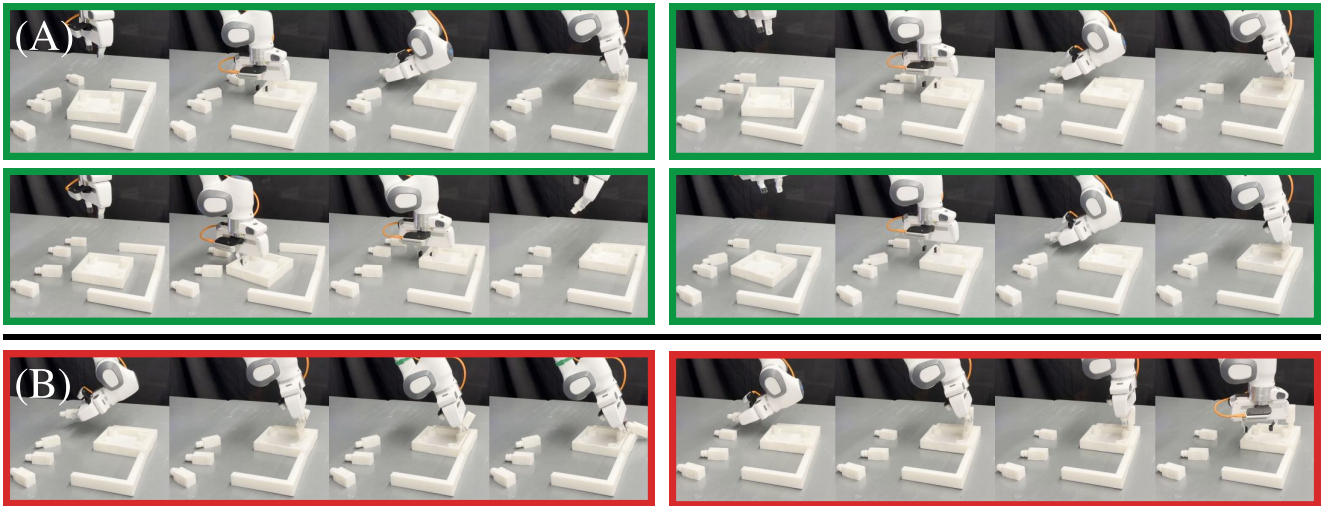


Fig. 10. (A) Examples of successful real world assembly from RGB. Co-training with simulation data reduces jerkiness and improves insertion robustness by containing a higher diversity of part poses and insertion locations (see Table II). (B) Example failure: difficulty adjusting the insertion angle/position when grasps lead to unseen in-hand part poses.

trained residual RL policy. We compare the co-trained policy to a baseline model trained only on real-world demonstrations. We compare the success rates achieved by each policy on two sets of 10 trials for the `one_leg` task. In the first set, we randomize part poses, while in the second set, we randomize obstacle poses (i.e., insertion location in the workspace).

The results, presented in Tab. II, show that incorporating simulation data improves real-world performance (e.g., increasing task completion rate from 20-30% to 50-60%). Qualitatively, the sim-to-real policy exhibits smoother behavior and makes fewer erratic movements that might exceed the robot’s physical limits. Fig. 10 shows examples of successful and unsuccessful task attempts.

To further probe the sim-to-real transfer and potential for acquiring new capabilities with the help of the simulator, we create a task variation where the part colors are changed from black to white. When rolling out the policy trained on real demos of white parts, the robot exhibits erratic behavior that caused the hardware to reach velocity limits on every trial we ran, as shown in Fig. 11 (A). When including synthetic data rendered with parts in black, the resulting policy can perform the task again (see Fig. 11). The resulting performance was still inferior to the performance on white parts, which motivates further work on closing the sim-to-real gap.

V. RELATED WORKS

a) Training diffusion models with reinforcement learning: The approach in [46,53] studied how to cast diffusion de-noising as a Markov Decision Process, enabling preference-aligned image generation with policy gradient RL. However, this method is unstable and hard to tune. [47] introduced a framework for direction diffusion policy fine-tuning which avoids this instability, but the method is architecture specific and does not introduce closed-loop

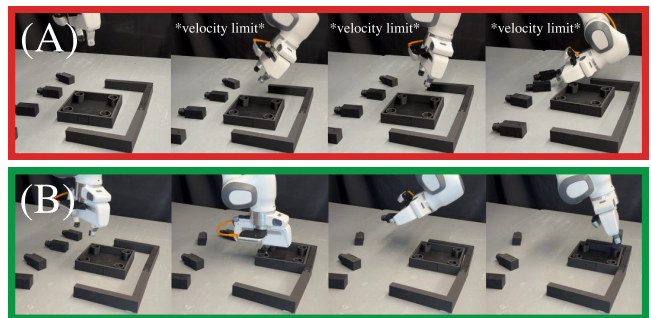


Fig. 11. (A) When changing the part appearances from white to black, the policy trained on real data only seizes to function. The behavior becomes erratic, and all trials ended with the robot hitting a velocity limit. (B) When mixing in synthetic data with more diverse colors (see Fig. 9), the policy regains the ability to complete the task, though with lower performance than for white parts.

control. Other ways to combine diffusion architectures with RL include Q-function-based importance sampling [55], advantage weighted regression [56], or changing the objective into a supervised learning problem with return conditioning [16,17,57]. Some have also explored augmenting the denoising training objective with a Q-function maximization objective [58] and iteratively changing the dataset with Q-functions [72]. Recent work developed techniques for training diffusion policies from scratch [54], leveraging unsupervised clustering and Q-learning combinations to encourage multi-modal behavior discovery. Our method avoids such complexity involved with directly optimizing diffusion models by using standard PPO to train simple residual policies that correct for errors made by the base policy.

b) Residual learning in robotics: Learning corrective residual components in conjunction with learned or

non-learned “base” models has been widely successful in robotics. Common frameworks include learning residual policies that correct for errors made by a nominal behavior policy [60,61,73]–[78] and combining learned components to correct for inaccuracies in analytical models for physical dynamics [79]–[81] or sensor observations [82]. Residual policies have been used in insertion applications [83], and recent work has applied residual policy learning to the same FurnitureBench task suite we study in this paper [84]. Their approach uses the residual component to model online human-provided corrections via supervised learning, whereas we train our residual policy from scratch with RL using task rewards in simulation.

VI. LIMITATIONS AND CONCLUSION

a) Limitations: The local nature of our residual policies is not well-suited for learning the macro-level behaviors required to recover from large-scale deviations like dropped parts. Our proposed method also struggles in regimes with very high initial scene randomness, as both the base policies and actions produced via RL exploration struggle to deal with out-of-support initial part poses. Furthermore, despite showcasing the advantage of incorporating simulation data, sim-to-real for RGB policies still presents a challenge. There remains a performance gap in both teacher-student distillation and sim-to-real distribution shifts. Future investigations may include better sim-to-real transfer techniques, exploration mechanisms for discovering how to correct large-scale execution errors, tractable interactive learning for real-world policy distillation, and incorporating inductive biases that help generalize to much broader initial state distributions.

b) Conclusion: This work presents `ResiP`, a simple yet effective approach for improving behavior-cloned policies on precise manipulation tasks using sparse rewards. Our key insight is recognizing modern chunked BC policies as trajectory planners that require closed-loop corrections for reliable execution. By training a residual policy with RL to provide these corrections, we sidestep the complexities of directly fine-tuning architectures like diffusion models while addressing fundamental limitations of BC – distribution shift and lack of reactivity.

Our results demonstrate that this approach significantly outperforms pure BC methods and direct RL fine-tuning across multiple challenging assembly tasks, improving success rates from $\sim 50\text{-}80\%$ to over 95% in many cases. Through careful ablations, we show the importance of both the fully closed-loop nature of the residual and the choice of a robust base policy, particularly for high-precision tasks like sub-millimeter insertions.

While we demonstrate successful real-world transfer through teacher-student distillation and sim-to-real co-training, the remaining performance gap suggests opportunities for improved sim-to-real procedures through direct vision-based RL or interactive distillation. Additionally, our results with different base architectures suggest this residual learning approach to be valuable for fine-tuning foundation models while preserving diverse capabilities.

ACKNOWLEDGMENTS

This work was partly supported by the Sony Research Award and the US Government. The computations in this paper were run on the FASRC cluster, supported by the FAS Division of Science Research Computing Group at Harvard University, and on the MIT Supercloud [85].

Author Contributions

Lars Ankile led the project and implemented most of the code and training infrastructure, including the main residual PPO implementation, and is the primary author.

Anthony Simeonov helped conceive of and advise on project goals, led deployment on real hardware and sim-to-real rendering, and helped write the paper.

Idan Shenfeld led the implementation of reinforcement learning baselines, helped debug residual PPO implementation, and helped write the paper.

Marcel Torne provided valuable insights, recommendations, and discussions on reinforcement learning fine-tuning and sim-to-real transfer.

Pulkit Agrawal advised the project and provided valuable feedback on project framing and contributions.

REFERENCES

- [1] S. Ross, G. Gordon, and D. Bagnell, "A reduction of imitation learning and structured prediction to no-regret online learning," in *Proceedings of the fourteenth international conference on artificial intelligence and statistics. JMLR Workshop and Conference Proceedings*, 2011, pp. 627–635.
- [2] K. Kimble, K. Van Wyk, J. Falco, E. Messina, Y. Sun, M. Shibata, W. Uemura, and Y. Yokokohji, "Benchmarking protocols for evaluating small parts robotic assembly systems," *IEEE robotics and automation letters*, vol. 5, no. 2, pp. 883–889, 2020.
- [3] F. Suárez-Ruiz and Q.-C. Pham, "A framework for fine robotic assembly," in *2016 IEEE international conference on robotics and automation (ICRA)*. IEEE, 2016, pp. 421–426.
- [4] Y. Lee, E. S. Hu, and J. J. Lim, "Ikea furniture assembly environment for long-horizon complex manipulation tasks," in *2021 IEEE international conference on robotics and automation (icra)*. IEEE, 2021, pp. 6343–6349.
- [5] M. Heo, Y. Lee, D. L. Kaist, and J. J. Lim, "FurnitureBench: Reproducible Real-World Benchmark for Long-Horizon Complex Manipulation," *RSS 2023*, 2023, arXiv: 2305.12821v1. [Online]. Available: <https://clvrai.com/furniture-bench>
- [6] T. Z. Zhao, V. Kumar, S. Levine, and C. Finn, "Learning Fine-Grained Bimanual Manipulation with Low-Cost Hardware," in *Proceedings of Robotics: Science and Systems*, Daegu, Republic of Korea, July 2023.
- [7] D. A. Pomerleau, "Alvinn: An autonomous land vehicle in a neural network," *Advances in neural information processing systems*, vol. 1, 1988.
- [8] S. Schaal, "Learning from Demonstration," in *Advances in Neural Information Processing Systems*, vol. 9. MIT Press, 1996. [Online]. Available: https://proceedings.neurips.cc/paper_files/paper/1996/hash/68d13cf26c4b4f4f932e3ef990093ba-Abstract.html
- [9] —, "Is imitation learning the route to humanoid robots?" *Trends in cognitive sciences*, vol. 3, no. 6, pp. 233–242, 1999.
- [10] N. Ratliff, J. A. Bagnell, and S. S. Srinivasa, "Imitation learning for locomotion and manipulation," in *2007 7th IEEE-RAS international conference on humanoid robots*. IEEE, 2007, pp. 392–397.
- [11] P. Agrawal, *Computational sensorimotor learning*. University of California, Berkeley, 2018.
- [12] T. Zhang, Z. McCarthy, O. Jow, D. Lee, X. Chen, K. Goldberg, and P. Abbeel, "Deep imitation learning for complex manipulation tasks from virtual reality teleoperation," in *2018 IEEE international conference on robotics and automation (ICRA)*. IEEE, 2018, pp. 5628–5635.
- [13] A. Brohan, N. Brown, J. Carbajal, Y. Chebotar, J. Dabis, C. Finn, K. Gopalakrishnan, K. Hausman, A. Herzog, J. Hsu *et al.*, "Rt-1: Robotics transformer for real-world control at scale," *arXiv preprint arXiv:2212.06817*, 2022.
- [14] E. Jang, A. Irpan, M. Khansari, D. Kappler, F. Ebert, C. Lynch, S. Levine, and C. Finn, "Bc-z: Zero-shot task generalization with robotic imitation learning," in *Conference on Robot Learning*. PMLR, 2022, pp. 991–1002.
- [15] M. Drolet, S. Stepputtis, S. Kailas, A. Jain, J. Peters, S. Schaal, and H. B. Amor, "A comparison of imitation learning algorithms for bimanual manipulation," *IEEE Robotics and Automation Letters*, 2024.
- [16] M. Janner, Y. Du, J. B. Tenenbaum, and S. Levine, "Planning with Diffusion for Flexible Behavior Synthesis," Dec. 2022, arXiv:2205.09991 [cs]. [Online]. Available: <http://arxiv.org/abs/2205.09991>
- [17] A. Ajay, Y. Du, A. Gupta, J. Tenenbaum, T. Jaakkola, and P. Agrawal, "Is Conditional Generative Modeling all you need for Decision-Making?" Jul. 2023, arXiv:2211.15657 [cs]. [Online]. Available: <http://arxiv.org/abs/2211.15657>
- [18] C. Chi, S. Feng, Y. Du, Z. Xu, E. Cousineau, B. Burchfiel, and S. Song, "Diffusion Policy: Visuomotor Policy Learning via Action Diffusion," Jun. 2023, arXiv:2303.04137 [cs]. [Online]. Available: <http://arxiv.org/abs/2303.04137>
- [19] T. Pearce, T. Rashid, A. Kanervisto, D. Bignell, M. Sun, R. Georgescu, S. V. Macua, S. Z. Tan, I. Momennejad, K. Hofmann, and S. Devlin, "Imitating Human Behaviour with Diffusion Models," Mar. 2023, arXiv:2301.10677 [cs, stat]. [Online]. Available: <http://arxiv.org/abs/2301.10677>
- [20] L. Lai, A. Z. Huang, and S. J. Gershman, "Action chunking as policy compression," *PsyArXiv*, 2022.
- [21] L. Ankile, A. Simeonov, I. Shenfeld, and P. Agrawal, "Juicer: Data-efficient imitation learning for robotic assembly," *arXiv preprint arXiv:2404.03729*, 2024.
- [22] S. Ross and D. Bagnell, "Efficient reductions for imitation learning," in *Proceedings of the thirteenth international conference on artificial intelligence and statistics. JMLR Workshop and Conference Proceedings*, 2010, pp. 661–668.
- [23] A. Yu, G. Yang, R. Choi, Y. Ravan, J. Leonard, and P. Isola, "Lucidsim: Learning agile visual locomotion from generated images," in *8th Annual Conference on Robot Learning*, 2024.
- [24] T. Z. Zhao, J. Tompson, D. Driess, P. Florence, S. K. S. Ghasemipour, C. Finn, and A. Wahid, "ALOHA unleashed: A simple recipe for robot dexterity," in *8th Annual Conference on Robot Learning*, 2024. [Online]. Available: <https://openreview.net/forum?id=gvdXE7ikHI>
- [25] J. Kober, J. A. Bagnell, and J. Peters, "Reinforcement learning in robotics: A survey," *The International Journal of Robotics Research*, vol. 32, no. 11, pp. 1238–1274, 2013.
- [26] J. Schulman, F. Wolski, P. Dhariwal, A. Radford, and O. Klimov, "Proximal Policy Optimization Algorithms," Aug. 2017, arXiv:1707.06347 [cs]. [Online]. Available: <http://arxiv.org/abs/1707.06347>
- [27] O. M. Andrychowicz, B. Baker, M. Chociej, R. Jozefowicz, B. McGrew, J. Pachocki, A. Petron, M. Plappert, G. Powell, A. Ray *et al.*, "Learning dexterous in-hand manipulation," *The International Journal of Robotics Research*, vol. 39, no. 1, pp. 3–20, 2020.
- [28] D. Kalashnikov, A. Irpan, P. Pastor, J. Ibarz, A. Herzog, E. Jang, D. Quillen, E. Holly, M. Kalakrishnan, V. Vanhoucke *et al.*, "Scalable deep reinforcement learning for vision-based robotic manipulation," in *Conference on robot learning*. PMLR, 2018, pp. 651–673.
- [29] G. B. Margolis, G. Yang, K. Paigwar, T. Chen, and P. Agrawal, "Rapid locomotion via reinforcement learning," *The International Journal of Robotics Research*, vol. 43, no. 4, pp. 572–587, 2024.
- [30] M. Torne, A. Simeonov, Z. Li, A. Chan, T. Chen, A. Gupta, and P. Agrawal, "Reconciling reality through simulation: A real-to-sim-to-real approach for robust manipulation," *arXiv preprint arXiv:2403.03949*, 2024.
- [31] T. Chen, M. Tippur, S. Wu, V. Kumar, E. Adelson, and P. Agrawal, "Visual dexterity: In-hand reorientation of novel and complex object shapes," *Science Robotics*, vol. 8, no. 84, p. eadc9244, 2023.
- [32] Y. Park, G. B. Margolis, and P. Agrawal, "Automatic environment shaping is the next frontier in rl," *arXiv preprint arXiv:2407.16186*, 2024.
- [33] A. Rajeswaran, V. Kumar, A. Gupta, G. Vezzani, J. Schulman, E. Todorov, and S. Levine, "Learning Complex Dexterous Manipulation with Deep Reinforcement Learning and Demonstrations," in *Proceedings of Robotics: Science and Systems (RSS)*, 2018.
- [34] S. James and A. J. Davison, "Q-attention: Enabling efficient learning for vision-based robotic manipulation," *IEEE Robotics and Automation Letters*, vol. 7, no. 2, pp. 1612–1619, 2022.
- [35] Y. Lu, K. Hausman, Y. Chebotar, M. Yan, E. Jang, A. Herzog, T. Xiao, A. Irpan, M. Khansari, D. Kalashnikov *et al.*, "Aw-opt: Learning robotic skills with imitation and reinforcement at scale," in *Conference on Robot Learning*. PMLR, 2022, pp. 1078–1088.
- [36] P. J. Ball, L. Smith, I. Kostrikov, and S. Levine, "Efficient online reinforcement learning with offline data," in *International Conference on Machine Learning*. PMLR, 2023, pp. 1577–1594.
- [37] S. Schaal, "Learning from demonstration," *Advances in neural information processing systems*, vol. 9, 1996.
- [38] A. Nair, B. McGrew, M. Andrychowicz, W. Zaremba, and P. Abbeel, "Overcoming exploration in reinforcement learning with demonstrations," in *2018 IEEE international conference on robotics and automation (ICRA)*. IEEE, 2018, pp. 6292–6299.
- [39] M. Nakamoto, S. Zhai, A. Singh, M. Sobol Mark, Y. Ma, C. Finn, A. Kumar, and S. Levine, "Cal-ql: Calibrated offline rl pre-training for efficient online fine-tuning," *Advances in Neural Information Processing Systems*, vol. 36, 2024.
- [40] I. Uchendu, T. Xiao, Y. Lu, B. Zhu, M. Yan, J. Simon, M. Bennice, C. Fu, C. Ma, J. Jiao *et al.*, "Jump-start reinforcement learning," in *International Conference on Machine Learning*. PMLR, 2023, pp. 34 556–34 583.
- [41] H. Hu, S. Mirchandani, and D. Sadigh, "Imitation bootstrapped reinforcement learning," *arXiv preprint arXiv:2311.02198*, 2023.
- [42] Q. Zheng, A. Zhang, and A. Grover, "Online decision transformer," in *international conference on machine learning*. PMLR, 2022, pp. 27 042–27 059.

- [43] J. Kober and J. Peters, "Imitation and reinforcement learning," *IEEE Robotics & Automation Magazine*, vol. 17, no. 2, pp. 55–62, 2010.
- [44] R. Ramrakhya, D. Batra, E. Wijmans, and A. Das, "Pirlnav: Pretraining with imitation and rl finetuning for objectnav," in *Proceedings of the IEEE/CVF Conference on Computer Vision and Pattern Recognition*, 2023, pp. 17 896–17 906.
- [45] A. Singh, H. Liu, G. Zhou, A. Yu, N. Rhinehart, and S. Levine, "Parrot: Data-driven behavioral priors for reinforcement learning," *arXiv preprint arXiv:2011.10024*, 2020.
- [46] K. Black, M. Janner, Y. Du, I. Kostrikov, and S. Levine, "Training diffusion models with reinforcement learning," *arXiv preprint arXiv:2305.13301*, 2023.
- [47] A. Z. Ren, J. Lidard, L. L. Ankile, A. Simeonov, P. Agrawal, A. Majumdar, B. Burchfiel, H. Dai, and M. Simchowitz, "Diffusion policy optimization," *arXiv preprint arXiv:2409.00588*, 2024.
- [48] Y. Narang, K. Storey, I. Akinola, M. Macklin, P. Reist, L. Wawrzyniak, Y. Guo, A. Moravanszky, G. State, M. Lu, A. Handa, and D. Fox, "Factory: Fast Contact for Robotic Assembly," in *Proceedings of Robotics: Science and Systems*, New York City, NY, USA, June 2022.
- [49] V. Makoviychuk, L. Wawrzyniak, Y. Guo, M. Lu, K. Storey, M. Macklin, D. Hoeller, N. Rudin, A. Allshire, A. Handa *et al.*, "Isaac gym: High performance gpu-based physics simulation for robot learning," *arXiv preprint arXiv:2108.10470*, 2021.
- [50] E. Todorov, T. Erez, and Y. Tassa, "Mujoco: A physics engine for model-based control," in *2012 IEEE/RSJ International Conference on Intelligent Robots and Systems*. IEEE, 2012, pp. 5026–5033.
- [51] R. Tedrake, *Robotic Manipulation*. Course Notes for MIT 6.421, 2024. [Online]. Available: <http://manipulation.mit.edu>
- [52] Y. Fan and K. Lee, "Optimizing ddpm sampling with shortcut finetuning," *arXiv preprint arXiv:2301.13362*, 2023.
- [53] Y. Fan, O. Watkins, Y. Du, H. Liu, M. Ryu, C. Boutilier, P. Abbeel, M. Ghavamzadeh, K. Lee, and K. Lee, "Dpok: Reinforcement learning for fine-tuning text-to-image diffusion models," 2023.
- [54] Z. Li, R. Krohn, T. Chen, A. Ajay, P. Agrawal, and G. Chalvatzaki, "Learning multimodal behaviors from scratch with diffusion policy gradient," 2024.
- [55] P. Hansen-Estruch, I. Kostrikov, M. Janner, J. G. Kuba, and S. Levine, "IDQL: Implicit Q-Learning as an Actor-Critic Method with Diffusion Policies," May 2023, arXiv:2304.10573 [cs]. [Online]. Available: <http://arxiv.org/abs/2304.10573>
- [56] W. Goo and S. Niekum, "Know your boundaries: The necessity of explicit behavioral cloning in offline rl," *arXiv preprint arXiv:2206.00695*, 2022.
- [57] L. Chen, K. Lu, A. Rajeswaran, K. Lee, A. Grover, M. Laskin, P. Abbeel, A. Srinivas, and I. Mordatch, "Decision transformer: Reinforcement learning via sequence modeling," *Advances in neural information processing systems*, vol. 34, pp. 15 084–15 097, 2021.
- [58] Z. Wang, J. J. Hunt, and M. Zhou, "Diffusion policies as an expressive policy class for offline reinforcement learning," *arXiv preprint arXiv:2208.06193*, 2022.
- [59] M. Wołczyk, B. Cupiał, M. Ostaszewski, M. Bortkiewicz, M. Zajkac, R. Pascanu, Ł. Kuciński, and P. Miłoś, "Fine-tuning reinforcement learning models is secretly a forgetting mitigation problem," *arXiv preprint arXiv:2402.02868*, 2024.
- [60] T. Silver, K. Allen, J. Tenenbaum, and L. Kaelbling, "Residual policy learning," *arXiv preprint arXiv:1812.06298*, 2018.
- [61] T. Davchev, K. S. Luck, M. Burke, F. Meier, S. Schaal, and S. Ramamoorthy, "Residual learning from demonstration: Adapting dmps for contact-rich manipulation," *IEEE Robotics and Automation Letters*, vol. 7, no. 2, pp. 4488–4495, 2022.
- [62] A. Nair, A. Gupta, M. Dalal, and S. Levine, "Awac: Accelerating online reinforcement learning with offline datasets," *arXiv preprint arXiv:2006.09359*, 2020.
- [63] A. Rajeswaran, V. Kumar, A. Gupta, G. Vezzani, J. Schulman, E. Todorov, and S. Levine, "Learning complex dexterous manipulation with deep reinforcement learning and demonstrations," *arXiv preprint arXiv:1709.10087*, 2017.
- [64] J. Lee, J. Hwangbo, L. Wellhausen, V. Koltun, and M. Hutter, "Learning quadrupedal locomotion over challenging terrain," *Science robotics*, vol. 5, no. 47, p. eabc5986, 2020.
- [65] A. Kumar, Z. Fu, D. Pathak, and J. Malik, "Rma: Rapid motor adaptation for legged robots," *arXiv preprint arXiv:2107.04034*, 2021.
- [66] M. Mittal, C. Yu, Q. Yu, J. Liu, N. Rudin, D. Hoeller, J. L. Yuan, R. Singh, Y. Guo, H. Mazhar, A. Mandekar, B. Babich, G. State, M. Hutter, and A. Garg, "Orbit: A unified simulation framework for interactive robot learning environments," *IEEE Robotics and Automation Letters*, vol. 8, no. 6, pp. 3740–3747, 2023.
- [67] S. Han, I. Shenfeld, A. Srivastava, Y. Kim, and P. Agrawal, "Value augmented sampling for language model alignment and personalization," 2024.
- [68] J. Song, C. Meng, and S. Ermon, "Denoising diffusion implicit models," *arXiv preprint arXiv:2010.02502*, 2020.
- [69] A. Kumar, A. Zhou, G. Tucker, and S. Levine, "Conservative q-learning for offline reinforcement learning," *Advances in Neural Information Processing Systems*, vol. 33, pp. 1179–1191, 2020.
- [70] J. Schulman, S. Levine, P. Abbeel, M. Jordan, and P. Moritz, "Trust region policy optimization," in *International conference on machine learning*. PMLR, 2015, pp. 1889–1897.
- [71] S. Ross, G. Gordon, and D. Bagnell, "A reduction of imitation learning and structured prediction to no-regret online learning," in *Proceedings of the fourteenth international conference on artificial intelligence and statistics*. JMLR Workshop and Conference Proceedings, 2011, pp. 627–635.
- [72] L. Yang, Z. Huang, F. Lei, Y. Zhong, Y. Yang, C. Fang, S. Wen, B. Zhou, and Z. Lin, "Policy representation via diffusion probability model for reinforcement learning," 2023.
- [73] J. Carvalho, D. Koert, M. Daniv, and J. Peters, "Residual robot learning for object-centric probabilistic movement primitives," *arXiv preprint arXiv:2203.03918*, 2022.
- [74] T. Johannink, S. Bahl, A. Nair, J. Luo, A. Kumar, M. Loskyll, J. A. Ojea, E. Solowjow, and S. Levine, "Residual reinforcement learning for robot control," in *2019 international conference on robotics and automation (ICRA)*. IEEE, 2019, pp. 6023–6029.
- [75] M. Alakuijala, G. Dulac-Arnold, J. Mairal, J. Ponce, and C. Schmid, "Residual reinforcement learning from demonstrations," *arXiv preprint arXiv:2106.08050*, 2021.
- [76] S. Haldar, J. Pari, A. Rai, and L. Pinto, "Teach a robot to fish: Versatile imitation from one minute of demonstrations," *arXiv preprint arXiv:2303.01497*, 2023.
- [77] S. Lee, Y. Wang, H. Etukuru, H. J. Kim, N. M. M. Shafullah, and L. Pinto, "Behavior generation with latent actions," *arXiv preprint arXiv:2403.03181*, 2024.
- [78] N. M. Shafullah, Z. Cui, A. A. Altanzaya, and L. Pinto, "Behavior transformers: Cloning k modes with one stone," *Advances in neural information processing systems*, vol. 35, pp. 22 955–22 968, 2022.
- [79] A. Ajay, J. Wu, N. Fazeli, M. Bauza, L. P. Kaelbling, J. B. Tenenbaum, and A. Rodriguez, "Augmenting physical simulators with stochastic neural networks: Case study of planar pushing and bouncing," in *2018 IEEE/RSJ International Conference on Intelligent Robots and Systems (IROS)*. IEEE, 2018, pp. 3066–3073.
- [80] A. Kloss, S. Schaal, and J. Bohg, "Combining learned and analytical models for predicting action effects from sensory data," *The International Journal of Robotics Research*, vol. 41, no. 8, pp. 778–797, 2022.
- [81] A. Zeng, S. Song, J. Lee, A. Rodriguez, and T. Funkhouser, "Tossing-bot: Learning to throw arbitrary objects with residual physics," *IEEE Transactions on Robotics*, vol. 36, no. 4, pp. 1307–1319, 2020.
- [82] E. Kaufmann, L. Bauersfeld, A. Loquercio, M. Müller, V. Koltun, and D. Scaramuzza, "Champion-level drone racing using deep reinforcement learning," *Nature*, vol. 620, no. 7976, pp. 982–987, 2023.
- [83] G. Schoettler, A. Nair, J. Luo, S. Bahl, J. A. Ojea, E. Solowjow, and S. Levine, "Deep reinforcement learning for industrial insertion tasks with visual inputs and natural rewards," in *2020 IEEE/RSJ International Conference on Intelligent Robots and Systems (IROS)*. IEEE, 2020, pp. 5548–5555.
- [84] Y. Jiang, C. Wang, R. Zhang, J. Wu, and L. Fei-Fei, "Transic: Sim-to-real policy transfer by learning from online correction," *arXiv preprint arXiv:2405.10315*, 2024.
- [85] A. Reuther, J. Kepner, C. Byun, S. Samsi, W. Arcand, D. Bestor, B. Bergeron, V. Gadepally, M. Houle, M. Hubbell, M. Jones, A. Klein, L. Milechin, J. Mullen, A. Prout, A. Rosa, C. Yee, and P. Michaleas, "Interactive Supercomputing on 40,000 Cores for Machine Learning and Data Analysis," in *2018 IEEE High Performance Extreme Computing Conference (HPEC)*, Sep. 2018, pp. 1–6, iSSN: 2377-6943. [Online]. Available: <https://ieeexplore.ieee.org/document/8547629>
- [86] Y. Zhou, C. Barnes, J. Lu, J. Yang, and H. Li, "On the continuity of rotation representations in neural networks," in *Proceedings of the IEEE/CVF conference on computer vision and pattern recognition*, 2019, pp. 5745–5753.

- [87] J. Schulman, P. Moritz, S. Levine, M. Jordan, and P. Abbeel, "High-dimensional continuous control using generalized advantage estimation," *arXiv preprint arXiv:1506.02438*, 2015.
- [88] K. He, X. Zhang, S. Ren, and J. Sun, "Deep residual learning for image recognition," in *Proceedings of the IEEE conference on computer vision and pattern recognition*, 2016, pp. 770–778.
- [89] S. Nair, A. Rajeswaran, V. Kumar, C. Finn, and A. Gupta, "R3M: A Universal Visual Representation for Robot Manipulation," Nov. 2022, arXiv:2203.12601 [cs]. [Online]. Available: <http://arxiv.org/abs/2203.12601>
- [90] J. Levinson, C. Esteves, K. Chen, N. Snavely, A. Kanazawa, A. Rostamizadeh, and A. Makadia, "An analysis of svd for deep rotation estimation," *Advances in Neural Information Processing Systems*, vol. 33, pp. 22 554–22 565, 2020.
- [91] A. R. Geist, J. Frey, M. Zobro, A. Levina, and G. Martius, "Learning with 3d rotations, a hitchhiker's guide to so(3)," 2024.
- [92] M. Reuss, M. Li, X. Jia, and R. Lioutikov, "Goal-Conditioned Imitation Learning using Score-based Diffusion Policies," Jun. 2023, arXiv:2304.02532 [cs]. [Online]. Available: <http://arxiv.org/abs/2304.02532>
- [93] B. Tang, M. A. Lin, I. Akinola, A. Handa, G. S. Sukhatme, F. Ramos, D. Fox, and Y. Narang, "Industreal: Transferring contact-rich assembly tasks from simulation to reality," in *Robotics: Science and Systems*, 2023.
- [94] X. Zhang, S. Jin, C. Wang, X. Zhu, and M. Tomizuka, "Learning insertion primitives with discrete-continuous hybrid action space for robotic assembly tasks," in *2022 International conference on robotics and automation (ICRA)*. IEEE, 2022, pp. 9881–9887.
- [95] O. Spector and D. Di Castro, "Insertionnet-a scalable solution for insertion," *IEEE Robotics and Automation Letters*, vol. 6, no. 3, pp. 5509–5516, 2021.
- [96] Y. Tian, K. D. Willis, B. A. Omari, J. Luo, P. Ma, Y. Li, F. Javid, E. Gu, J. Jacob, S. Sueda *et al.*, "Asap: Automated sequence planning for complex robotic assembly with physical feasibility," *arXiv preprint arXiv:2309.16909*, 2023.
- [97] H. Hu, S. Mirchandani, and D. Sadigh, "Imitation Bootstrapped Reinforcement Learning," Nov. 2023, arXiv:2311.02198 [cs]. [Online]. Available: <http://arxiv.org/abs/2311.02198>
- [98] J. Luo, Z. Hu, C. Xu, Y. L. Tan, J. Berg, A. Sharma, S. Schaal, C. Finn, A. Gupta, and S. Levine, "SERL: A Software Suite for Sample-Efficient Robotic Reinforcement Learning," Jan. 2024, arXiv:2401.16013 [cs]. [Online]. Available: <http://arxiv.org/abs/2401.16013>
- [99] L. Ouyang, J. Wu, X. Jiang, D. Almeida, C. Wainwright, P. Mishkin, C. Zhang, S. Agarwal, K. Slama, A. Ray *et al.*, "Training language models to follow instructions with human feedback," *Advances in neural information processing systems*, vol. 35, pp. 27 730–27 744, 2022.

APPENDIX I
IMPLEMENTATION DETAILS

A. Training Hyperparameters

a) *State-based behavior cloning*: We provide a detailed set of hyperparameters used for training. General hyperparameters for all models can be found in [Tab. III](#), while specific hyperparameters for the diffusion models are in [Tab. IV](#), and those for the MLP baseline are in [Tab. V](#).

TABLE III. Training hyperparameters shared for all state-based BC models

Parameter	Value
Control mode	Absolute end-effector pose
Action space dimension	10
Proprioceptive state dimension	16
Orientation Representation	6D [86]
Max LR	10^{-4}
LR Scheduler	Cosine
Warmup steps	500
Weight Decay	10^{-6}
Batch Size	256
Max gradient steps	400k

TABLE IV. State-based diffusion pre-training hyperparameters

Parameter	Value
U-Net Down dims	[256, 512, 1024]
Diffusion step embed dim	256
Kernel size	5
N groups	8
Parameter count	66M
Observation Horizon T_o	1
Prediction Horizon T_p	32
Action Horizon T_a	8
DDPM Training Steps	100
DDIM Inference Steps	4

TABLE V. State-based MLP pre-training hyperparameters

Parameter	Value
Residual Blocks	5
Residual Block Width	1024
Layers per block	2
Parameter count	11M
Observation Horizon T_o	1
Prediction Horizon T_p (S / C)	1 / 8
Action Horizon T_a (S / C)	1 / 8

b) *State-based reinforcement learning*: Below, we list the hyperparameters used for online reinforcement learning fine-tuning. The parameters that all state-based RL methods shared are in [Tab. VI](#). Method-specific hyperparameters for training the different methods are in the tables below, direct fine-tuning of the MLP in [Tab. VII](#), online IDQL in [Tab. VIII](#), and the residual policy in [Tab. IX](#). The different methods were tuned independently, but the same hyperparameters were used for all tasks within each method.

TABLE VI. Hyperparameters shared for all online fine-tuning approaches

Parameter	Value
Control mode	Absolute end-effector pose
Action space dimension	10
Proprioceptive state dimension	16
Orientation Representation	6D [86]
Num parallel environments	1024
Max environment steps	500M
Critic hidden size	256
Critic hidden layers	2
Critic activation	ReLU
Critic last layer activation	Linear
Critic last layer bias initialization	0.25
Discount factor	0.999
GAE [87] lambda	0.95
Clip ϵ	0.2
Max gradient norm	1.0
Target KL	0.1
Num mini-batches	1
Episode length, <code>one_leg</code>	700
Episode length, <code>lamp/round_table</code>	1000
Normalize advantage	true

TABLE VII. Hyperparameters for direct fine-tuning of MLP

Parameter	Value
Update epochs	1
Learning rate actor	10^{-4}
Learning rate critic	10^{-4}
Value function loss coefficient	1.0
KL regularization coefficient	0.5
Actor Gaussian initial log st.dev.	-4.0

TABLE VIII. Hyperparameters for training value-augmented diffusion sampling (IDQL)

Parameter	Value
Update epochs	10
Learning rate Q-function	10^{-4}
Learning rate scheduler	Cosine
Num action samples	20
Actor added Gaussian noise, log st.dev.	-4

TABLE IX. Hyperparameters for residual PPO training

Parameter	Value
Residual action scaling factor	0.1
Update epochs	50
Learning rate actor	$3 \cdot 10^{-4}$
Learning rate critic	$5 \cdot 10^{-3}$
Learning rate scheduler	Cosine
Value function loss coefficient	1.0
Actor Gaussian initial log st.dev.	-1.0

c) Image-based real-world distillation: For the real-world experiments, we use a separate set of hyperparameters, presented in [Tab. X](#). The main difference is that we found in experimentation that the transformer backbone in [18] worked better than the UNet for real-world experiments. These models are also operating from RGB observations instead of privileged states, and we provide parameters for the image augmentations applied to the front camera in [Tab. XI](#) and the wrist camera in [Tab. XII](#).

TABLE X. Training hyperparameters for real-world distilled policies

Parameter	Value
Control mode	Absolute end-effector pose
Action space dimension	10
Proprioceptive state dimension	16
Orientation Representation	6D [86]
Max policy LR	10^{-4}
Max encoder LR	10^{-5}
LR Scheduler (both)	Cosine
Policy scheduler warmup steps	1000
Policy scheduler warmup steps	5000
Weight decay	10^{-3}
Batch size	256
Max gradient steps	500k
Image size input	$2 \times 320 \times 240 \times 3$
Image size encoder	$2 \times 224 \times 224 \times 3$
Vision Encoder Model	ResNet18 [88]
Encoder Weights	R3M [89]
Encoder Parameters	2×11 million
Encoder Projection Dim	128
Diffusion backbone architecture	Transformer (similar to [18])
Transformer num layers	8
Transformer num heads	4
Transformer embedding dim	256
Transformer embedding dropout	0.0
Transformer attention dropout	0.3
Transformer causal attention	true

TABLE XI. Parameters for front camera image augmentation

Parameter	Value
Color jitter (all parameters)	0.3
Gaussian blur, kernel size	5
Gaussian blur, sigma	(0.01, 1.2)
Random crop area	280×240
Random crop size	224×224
Random erasing, fill value	random
Random erasing, probability	0.2
Random erasing, scale	(0.02, 0.33)
Random erasing, ratio	(0.3, 3.3)

TABLE XII. Parameters for wrist camera image augmentation

Parameter	Value
Color jitter (all parameters)	0.3
Gaussian blur, kernel size	5
Gaussian blur, sigma	(0.01, 1.2)
Random crop	Not used
Image resize	$320 \times 240 \rightarrow 224 \times 224$

B. Action and State-Space Representations

a) Action space: The policies predict 10-dimensional actions consisting of absolute poses in the robot base frame as the actions and a gripper action. In particular, the first 3 dimensions predict the desired end-effector position in the workspace, the next 6 predict the desired orientation using a 6-dimensional representation described below. The final dimension is a gripper action, 1 to command closing gripper and -1 for opening.

b) Proprioceptive state space: The policy receives a 16-dimensional vector containing the current end-effector state and gripper width. In particular, the first 3 dimensions is the current position in the workspace, the next 6 the current orientation in the base frame (the same 6D representation), the next 3 the current positional velocity, the next 3 the current roll, pitch, and yaw angular velocity, and finally the current gripper width.

c) Rotation representation: We use a 6D representation to represent all orientations and rotations for the predicted action, and proprioceptive end-effector pose orientation [86,90]. The poses of the parts in state-based environments are represented with unit quaternions. While this representation contains redundant dimensions, it is continuous, meaning that small changes in orientation lead to small changes in the representation values, which can make learning easier [86,90,91].

This is not generally the case for Euler angles and quaternions. The 6D representation is constructed by taking two arbitrary 3D vectors and performing Gram-Schmidt orthogonalization to obtain a third orthogonal vector to the first two. The resulting three orthogonal vectors form a rotation matrix that represents the orientation. The end-effector rotation angular velocity is still encoded as roll, pitch, and yaw values.

d) Action and state-space normalization: All dimensions of the action, proprioceptive state, and parts pose (for state-based environments), were independently scaled to the range $[-1, 1]$. That is, we did not handle orientation representations (quaternions/6D [86]) in any particular way. The normalization limits were calculated over the dataset at the start of behavior cloning training. They were stored in the actor with the weights and reused as the normalization limits when training with reinforcement learning. The normalization used here follows the same approach as in previous works such as [18,92]. This normalization method is widely accepted for diffusion models. In [92], the input was standardized to have a mean of 0 and a standard deviation of 1, instead of using min-max scaling to the range of $[0, 1]$. This approach was not tested in our experiments.

C. Image Augmentation

During training, we apply image augmentation and random cropping to both camera views. Specifically, only the front camera view undergoes random cropping. We also apply color jitter with a hue, contrast, brightness, and saturation set to 0.3. Additionally, we apply Gaussian blur with a kernel size of 5 and sigma between 0.1 and 5 to both camera views.

At inference time, we statically center-crop the front camera image from 320x240 to 224x224 and resize the wrist camera view to the same dimensions. For both the random and center crops, we resized the image to 280x240 to ensure that essential parts of the scene are not cropped out due to excessive movement.

The values mentioned above were chosen based on visual assessment to balance creating adversarial scenarios and keeping essential features discernible. We have included examples of these augmentations below.

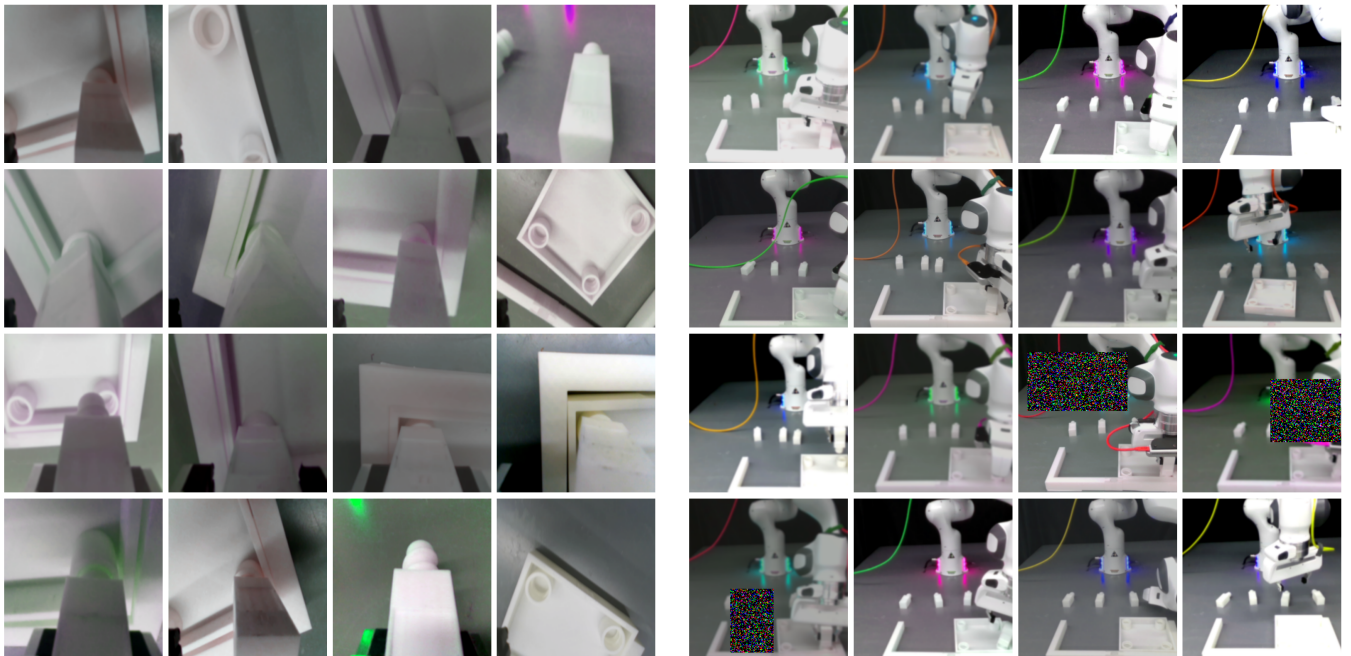


Fig. 12. **Left:** Examples of augmentations of the wrist camera view, consisting of color jitter and Gaussian blur. **Right:** Examples of augmentations for the front view also consist of color jitter and Gaussian blur augmentations and random cropping.

APPENDIX II TASKS AND ENVIRONMENT

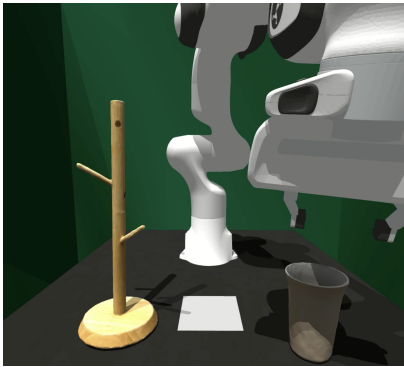
A. Tasks details and reward signal

a) Furniture assembly tasks: We detail a handful of differentiating properties for each of the three tasks we use in Tab. XIII. `one_leg` involves assembling 2 parts, the tabletop and one of the 4 table legs. The assembly is characterized as successful if the relative poses between the parts are close to a predefined assembled relative pose. When this pose is achieved, the environment returns a reward of 1. That is, for the `one_leg` task, the policy received a reward of 1 only at the very end of the episode. For `round_table` and `lamp`, which consists of assembling 3 parts together, the policy receives

a reward signal of 1 for each pair of assembled parts. E.g. for the `lamp` task, when the bulb is fully screwed into the base, the first reward of 1 is received, and the second is received when the shade is correctly placed.

b) Real-to-sim task: `mug-rack`: This task involves the robot picking up a coffee mug and hanging it by the handle on one of two pegs on a rack. See Fig. 13 for task illustration. This task is interesting for two main reasons. First, we don't have any CAD models for the objects. Instead, we used scanned imports of real-world objects (obtained with the ARCode app on the iPhone App Store). Second, the task has inherent multi-modality in that the mug can be hung in one of two ways for each of the two pegs.

The diffusion and residual policy system works well for this task. First, the base diffusion model captures the task's multimodality and sometimes hangs the mug on both pegs. Furthermore, the residual RL procedure keeps this multimodality intact as the base model is frozen.



(a) Example task initialization of the `mug-rack` task.



(b) Example of hanging the mug on the lower rack.

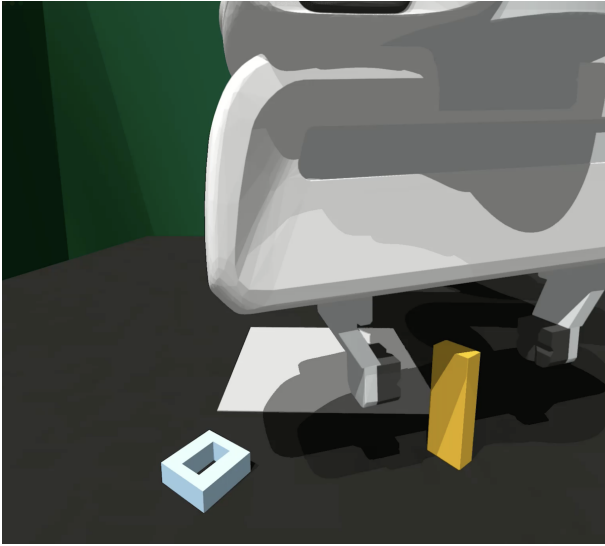


(c) Example of hanging the mug on the upper rack.

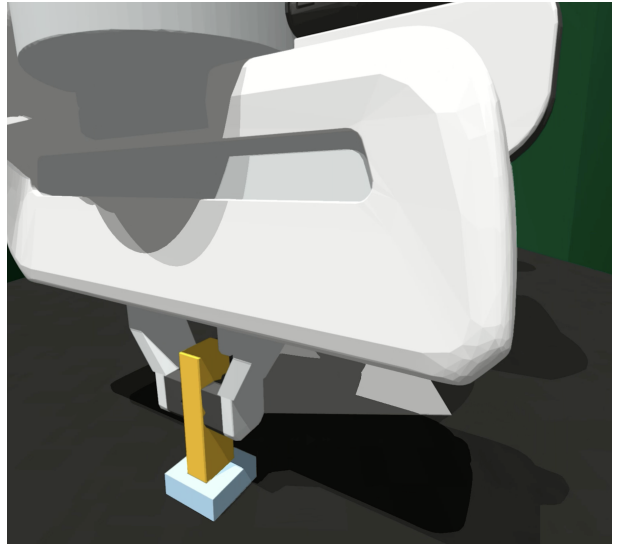
Fig. 13. Overview of the new `mug-rack` task we add to showcase the real-to-sim capabilities that one can leverage in tandem with our pipeline. This also shows how reward signals can be inferred directly from data instead of being hand-designed. Finally, as the task can be completed in one of several ways, this task also tests the policies' capability to deal with multi-modality in the task.

c) High-precision, Factory task: `peg-in-hole`: To push the limits of precision in simulation, controller, and policy, we pick one of the insertion tasks from the Factory task suite [48], which involves grasping a peg and inserting it in a hole with a 0.2mm clearance, i.e., 25x tighter than the FurnitureBench [5] tasks. See Fig. 14 for task illustration.

Our approach also worked out of the box on this task, using the same hyperparameters as for the FurnitureBench tasks. Here, we achieve 5% success rate in pre-training and $\sim 99\%$ in fine-tuning. Good performance at this task is essentially entirely dominated by the ability to locally adjust the peg until it lines up with the hole, and the high final success rate achieved by our approach reflects that the local nature of the corrections learned by our residual policy is well aligned with such task scenarios.



(a) Example task initialization of the `peg-in-hole` task.



(b) Example of task completion when the peg is fully inserted.

Fig. 14. Overview of the new `peg-in-hole` task we add to push the requirement for precision. We find that the pipeline as presented works well with the same hyperparameters used for the furniture tasks.

TABLE XIII. Task Attribute Overview

	<code>one_leg</code>	<code>round_table</code>	<code>lamp</code>	<code>mug-rack</code>	<code>peg-in-hole</code>	<code>biman-insert</code>
Mean episode length	~500	~700	~600	~150	~200	~400
# Parts to assemble	2	3	3	2	2	2
Num rewards	1	2	2	1	1	1
Dynamic object	✗	✗	✓	✗	✗	✗
# Precise insertions	1	2	1	0	1	1
# Screwing sequences	1	2	1	0	0	0
Precise grasping	✗	✓	✗	✗	✗	✗
Insertion occlusion	✗	✓	✗	✓	✗	✗
Control frequency	10 Hz	10 Hz	10 Hz	10 Hz	10 Hz	50 Hz
Degrees-of-Freedom	7	7	7	7	7	14

B. Details on randomization scheme

The “low” and “medium” randomness settings we used for data collection and evaluation reflect how much the initial part poses may vary when the environment is reset. We tuned these conditions to mimic the levels of randomness introduced in the original FurnitureBench suite [5]. However, we found that their method of directly sampling random poses often leads to initial part configurations colliding, requiring expensive continued sampling to eventually find an initial layout where all parts do not collide.

Our modified randomization scheme instead initializes parts to a single pre-specified set of feasible configurations. Then, it applies a randomly sampled force and torque to each part (where the force/torque magnitudes are tuned for each part and scaled based on the desired level of randomness). This scheme allows the physics simulation to ensure parts stay out of collision while providing a controlled amount of variation in the initial scene randomness.

The second way we modified the randomization scheme was to randomize the position of the U-shaped obstacle fixture and the parts (the obstacle fixture was always kept in a fixed position in [5]). We reasoned that, for visual sim-to-real without known object poses, we could only imperfectly and approximately align the obstacle location in the simulated and real environment. Rather than attempting to make this alignment perfect, we instead trained policies to cover some range of possible obstacle locations, hoping that the real-world obstacle position would fall within the distribution the policies have seen in simulation. Fig. 15 shows examples of our different randomness levels for each task in simulation.

C. Adjustments to FurnitureBench simulation environments

In addition to our modified force-based method of controlling the initial randomness, we introduced multiple other modifications to the original FurnitureBench environments proposed in [5] to enable the environment to run fast enough to be feasible for online RL training. With these changes, we could run at a total of ~4000 environment steps per second across 1024 parallel environments. The main changes are listed below:



Fig. 15. Examples of initial scene layouts for one_leg, lamp, and round_table with different levels of initial part pose and obstacle fixture randomness

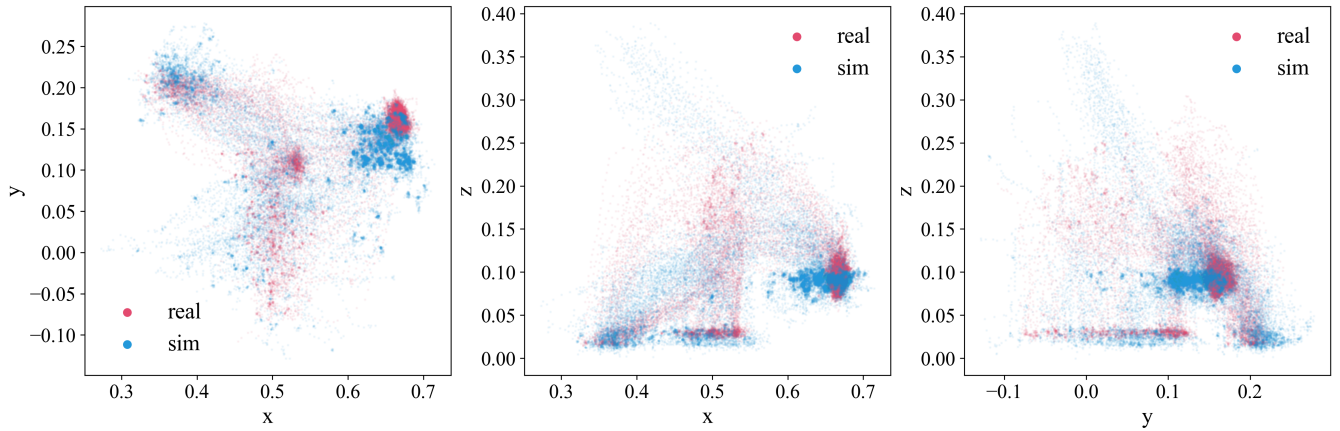


Fig. 16. Plots of the x, y, z action coordinates in the demo datasets for the `one_leg` task in the real world and the simulator. That is, each dot represents one action from one of the 40/50 trajectories. Red is from real-world demos, and blue is from the simulator. **Left:** Top-down view, showing the x, y positions in the workspace visited. In the top right, the insertion point is shown, where we see that the simulator has a wider distribution but could have covered better in the positive y -direction. **Middle:** Side-view of the actions taken in the x, z plane. The insertion point is to the right in the plot; again, we see more spread in the simulation data. **Right:** Front view of the y, z actions.

- 1) Vectorized reward computation, done check, robot, part, and obstacle resets, and differential inverse kinematics controller.
- 2) Removed April tags from 3D models to ensure vision policies would not rely on tags to complete the tasks. We tried to align with the original levels of randomness, but only to an approximation.
- 3) Deactivate camera rendering when running the environment in state-only mode.
- 4) Correct an issue where the physics was not stepped a sufficient amount of time for sim time to run at 10Hz, and subsequently optimize calls to fetch simulation results, stepping of graphics, and refreshing buffers.
- 5) Artificially constrained bulb from rolling on the table until robot gripper is nearby as the rolling in the simulator was exaggerated compared to the real-world parts.

APPENDIX III RGB SIM2REAL TRANSFER

a) Visualization of overlap in action space in real and sim: For data from the simulation to be useful for *increasing* the support of the policy for real-world deployment, we posit that it needs to *cover* the real-world data. We visualize the distributions of actions in the training data in Fig. 16. Since actions are absolute poses in the robot base frame, we can take the x, y, z coordinates for all actions from simulation and real-world demonstration data and plot them. Each of the 3 plots is a different cross-section of the space, i.e., a view from top-down, side, and front. In general, we see that the simulation action distribution is more spread out and mostly covers real-world actions.

b) Visual Domain randomization: In addition to randomizing part poses and the position of the obstacle, we randomize parts of the rendering which is not easily randomized by simple image augmentations, like light placement (changing shadows), camera pose, and individual part colors. See Fig. 17 for examples of front-view images obtained from our domain randomization and re-rendering procedure.

APPENDIX IV VISUALIZATION OF RESIDUAL POLICY ACTIONS

We hypothesize that the strength of the residual policy is that it can operate locally and make corrections to the base action predicted by the pretrained policy operating on the macro scale in the scene. We show an example of this behavior in Fig. 18. Here, we visualize the base action with the red line, the correction predicted by the residual in blue, and the net action of the combined policy in green.

We find that the residual has indeed learned to correct the base policy’s actions, which often leads to failure. One common example is for the base policy to be imprecise in the approach to the hole during insertion, pushing down with the peg not aligned with the hole, causing the peg to shift in the gripper, which leads to a grasp-pose unseen in the training data and the policy inevitably fails. The residual policy counteracts the premature push-down and correct the placement towards the hole, improving task success. See video examples of this behavior on the accompanying website: <https://residual-assembly.github.io/>.

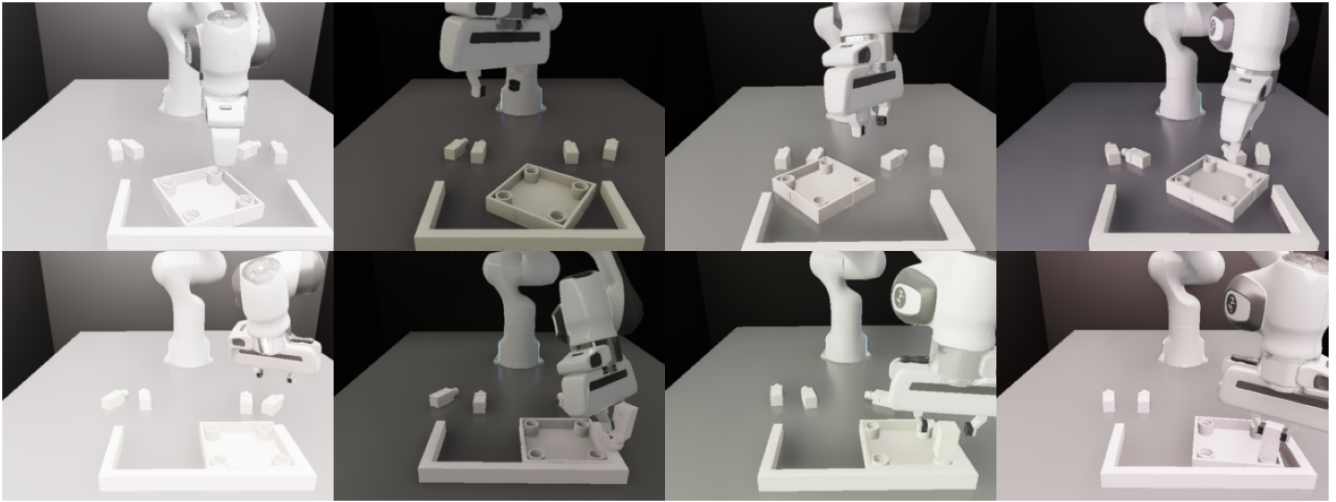


Fig. 17. Examples of the randomization applied when rendering out the simulation trajectories used for co-training for the real-world policies.

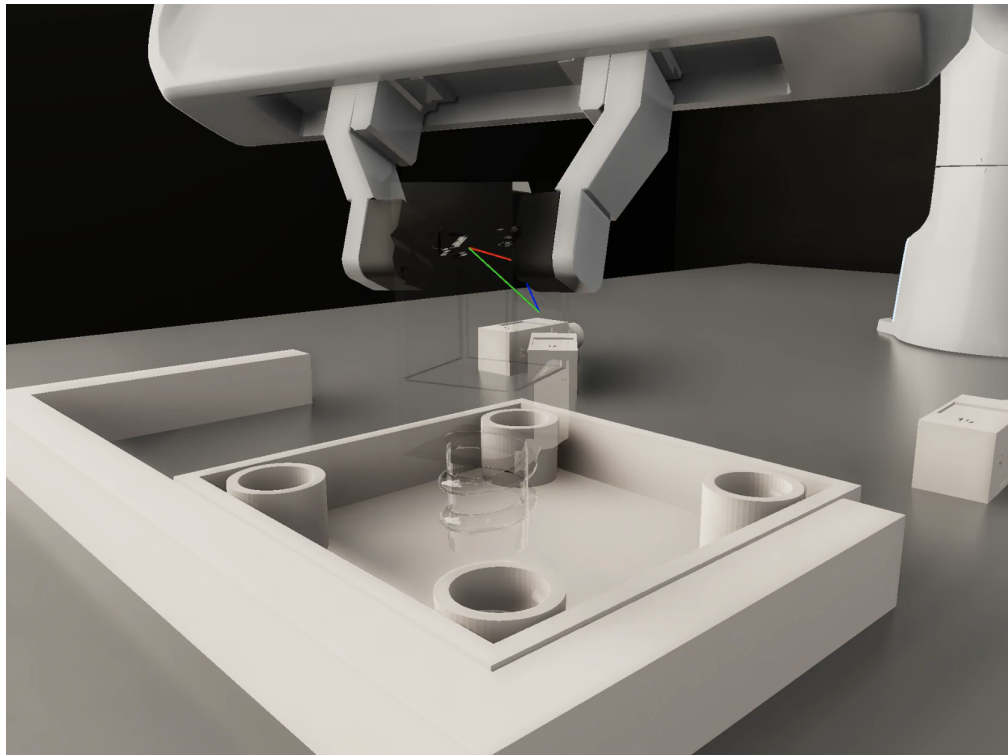


Fig. 18. Visualization of the effect of the residual policy during insertion, the phase requiring the most precision. The red line shows the action commanded by the base policy. The blue is the correction predicted by the residual, and the green is the net action. The residual learns to correct actions that typically lead to failure.

APPENDIX V
REAL-WORLD RESULTS

A. Quantitative Results Failure Mode Breakdown

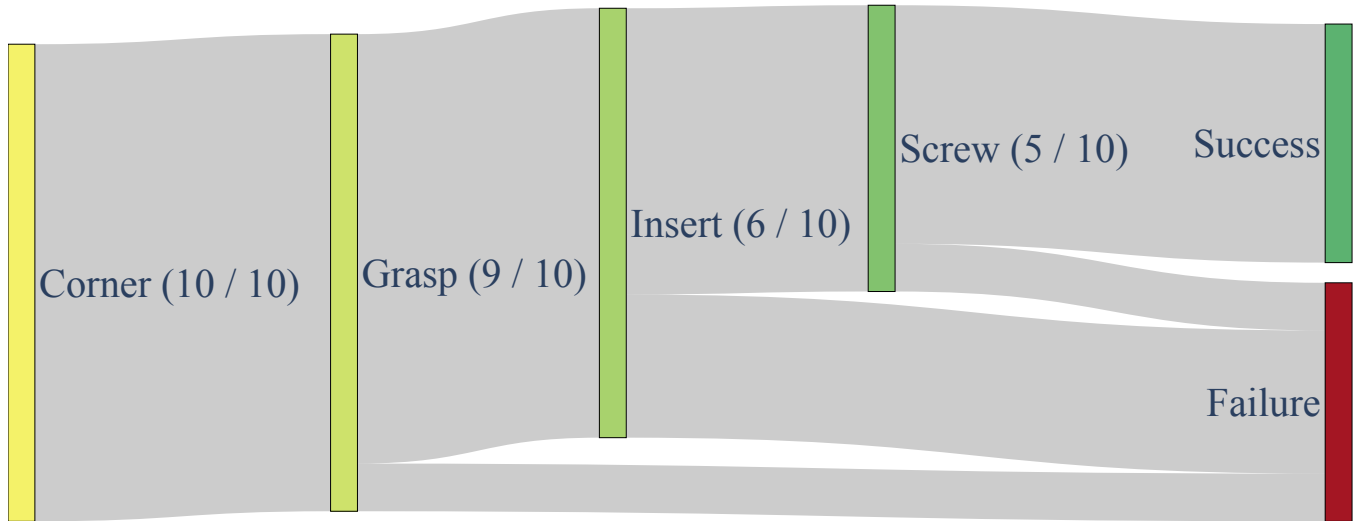


Fig. 19. Sankey diagram for the success rate and failure points for the real-world rollouts with 40 real and 350 simulation demos.

The diagram in Fig. 19 shows how successful and failed completion of individual sub-skills along the `one_leg` task amount to our overall final success rates reported in Tab. II (bottom row, corresponding to “40 real + 350 sim” with random initial part poses and a fixed obstacle pose).

B. Extension of Pipeline to Unseen Settings

Here, we conduct further qualitative experiments to evaluate whether our simulation-based co-training pipeline can make policies more robust to real-world parts with visual appearances that are unseen in real world demos. To test this, we 3D printed the same set of parts used in the `one_leg` task in black, and rolled out various policies on these black parts (rather than the white-colored parts used throughout our other experiments). This setting is especially relevant in industrial domains where parts can come in a variety of colors to which the assembly system must be invariant (e.g., the same piece of real-world furniture usually comes in many colors).

When deploying the policy trained on the same 40 demos as in the main experiment, which only had *white*, the policy cannot come close to completing the task. The behavior is highly erratic and triggered the velocity limits of the Franka on every trial we ran. We compare this baseline policy trained on differently colored parts to a policy co-trained on both real and synthetic data from simulation. However, when creating the synthetic dataset for this test, we added in additional randomization of part color, with an emphasis on black or gray colors in this case, as shown in Fig. 21. When we co-train a policy on a mix of the same real-world demos containing *only* white parts as before, with a dataset of 400 synthetic demos with *varying* part colors, the resulting policy can complete the task, as illustrated in Fig. 21 (and even when it fails at the entire task sequence, the predicted motions are much more reasonable than the erratic policy which has overfit to real-world parts of a specific color).

For example videos, please see the accompanying website: <https://residual-assembly.github.io/>. We note, however, that the resulting policy is considerably less reliable than the corresponding policy rolled out with white parts, which illustrates that there is still a meaningful sim2real gap.

APPENDIX VI
EXPANDED RELATED WORK

a) *Learning robotic assembly skills:* Robotic assembly has been used by many as a problem setting for various behavior learning techniques [61,93]–[96]. Enabling assembly that involves multi-skill sequencing (e.g., fixturing → grasping → insertion → screwing) directly from RGB images has remained challenging, especially *without* explicitly defining sub-skill-specific boundaries and supervision. Concurrent work [84] explores a similar framework to ours on FurnitureBench tasks [5], but instead supervises learned policies on a per-skill basis and incorporates 3D point clouds. IndustReal [93] also leverages RL in simulation to train high-precision skills for tight-tolerance part insertion in the real world. However, they train their RL

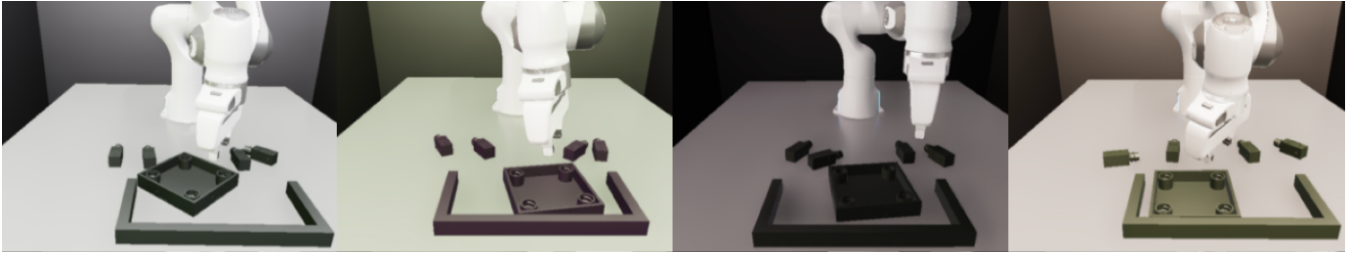


Fig. 20. Randomizing the visual appearance of the scene in the simulator allows for more fine-grained control and varying attributes that are hard to isolate in standard image augmentation techniques. Here, we illustrate how we can easily cover a larger space of part appearances without jittering the colors of everything else in tandem.

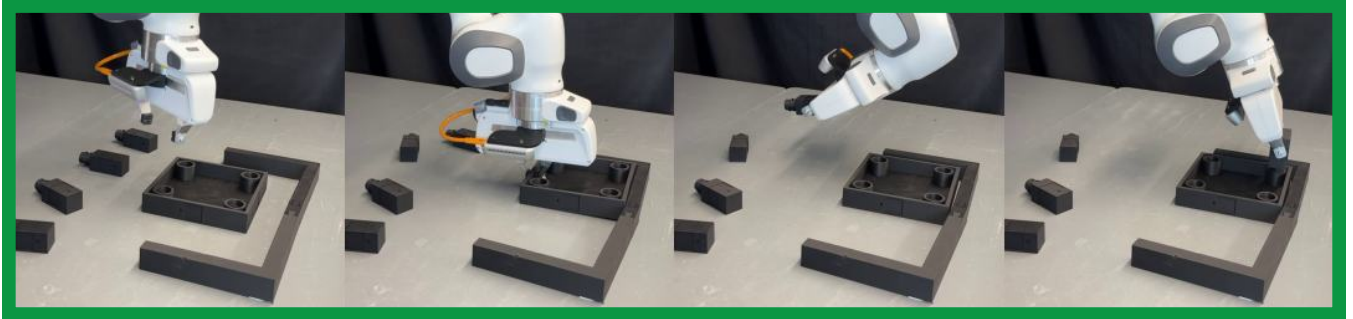


Fig. 21. An example of a successful rollout of a policy co-trained on 40 real-world demos containing only white parts and 400 synthetic demos with part colors randomized.

policies from scratch using carefully-designed shaped rewards and curricula, whereas we bootstrap RL from BC pre-training, which enables RL to operate with simple sparse rewards for achieving the desired assembly.

b) Complementary combinations of behavior cloning and reinforcement learning: Various combinations of learning from demonstrations/behavior cloning and reinforcement learning have begun maturing into standard tools in the learning-based control development paradigm [33,35]. For instance, demonstrations are often used to support RL in overcoming exploration difficulty and improving sample efficiency [30,97,98]. RL can also act as a robustification operator to improve upon base BC behaviors [30,35], paralleling the RL fine-tuning paradigm that has powered much of the recent advancement in other areas like NLP [99] and vision [46]. Additionally, many successful robotics deployments [31,64,65] have been powered by the “teacher-student distillation” paradigm, wherein perception-based “student” policies are trained to clone behaviors produced by a state-based “teacher” policy, which is typically trained via RL in simulation. We demonstrate that our residual RL approach for fine-tuning modern diffusion policy architectures can allow each of these complementary ways to combine BC and RL to come together and enable precise manipulation directly from RGB images.

APPENDIX VII

EXTENDED LIMITATIONS AND FURTHER WORK

a) Real-world distillation: Our experiments have demonstrated the effectiveness of online learning versus offline or passive learning through behavior cloning. Still, we employ only offline learning in our teacher-student distillation phase for sim-to-real transfer, which will likely upper-bound the performance we can transfer to the real world. Combining our pipeline with techniques for online learning could improve performance significantly. However, at this point, there are significant challenges to overcome to make this practically applicable to the tasks studied herein.

The field is progressing rapidly, and we are excited to investigate how online learning in the real world can be made practical for a broader set of tasks with longer horizons and less obvious ways of performing automatic state resets in follow-up work. This effort further ties into a more general framework for pre-training and adaptation of robot systems where the deployed robot can continue learning and adapting “on the job” after deployment. These investigations complement the methods presented in this paper and are not in scope.

At the same time, our results indicate that making more capable systems only through increasing the collection of real-world demos may also be fundamentally limited unless online learning is introduced as a fine-tuning step in those systems.

b) Locality of online correction learning: Though effective, we re-emphasize that our residual online reinforcement learning framework has the fundamental limitation of being bound to the pre-trained policy and mainly performing locally corrective actions. This limitation is both a strength and a weakness. First, the strong pre-trained prior allows RL to perform

the tasks and improve, and having a frozen prior helps stabilize training and prevent collapse. At the same time, the degree to which online learning can generalize to states far from the training set is limited.

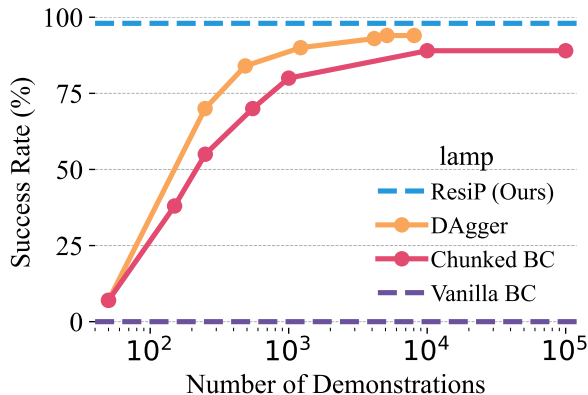
c) Limitations of simulators in contact-rich tasks: We have added an experiment for a task from the Factory [48] task suite that pushes the accuracy of the simulator more than with the original FurnitureBench [5] tasks. This new task has a clearance of 0.2mm for the insertion, which shows that the general BC + Residual RL framework also works well in this setting. We did not show, however, that this transfers to the real world, and it would likely be more challenging than in the original tasks for at least two reasons. First, with increased precision requirements, accurate calibration of physics parameters between the actual and simulated environment will likely matter more. Second, performing manipulation from vision when parts are smaller is more challenging.

APPENDIX VIII

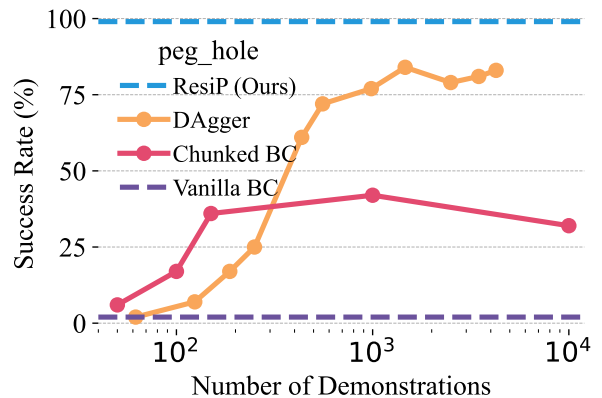
FURTHER ANALYSIS OF OFFLINE VERSUS ONLINE LEARNING

A. Distillation scaling analysis

The scaling analyses in Fig. 22 show the same trends as in Fig. 1 (right) and Fig. 7 for the tasks `lamp` and `peg-in-hole`. We believe that this data point suggests that pure offline learning from demonstrations may not be sufficient for policies to learn robust and reactive policies, pointing towards the necessity for techniques like RL to reach a high level of robustness and reliability.



(a) Scaling analysis for the `lamp` task. This task appears significantly more conducive to offline learning than the other tasks tested.



(b) Success rates in exploration phase of training for `one_leg`, low randomness.

Fig. 22. We run similar scaling analyses as in Fig. 1 (right) and Fig. 7 for `lamp` and `peg-in-hole`. The general findings of interactive learning are that it is more efficient and has higher asymptotical performance. However, the difference appears to be much smaller for `lamp` and bigger for `peg-in-hole`. What drives these differences are left for future work.

B. Interactive distillation with DAgger

DAgger [1] can learn from scratch significantly more efficiently than pure BC measured in both gradient steps and samples. We have added the DAgger performance to the scaling plot, shown in orange in Fig. 22. Consider the scaling plot in Fig. 1 (right) as an example. In $\sim 10k$ gradient steps, DAgger surpasses BC from 50 human demos trained with $\sim 100k$ steps. After 10k steps, it has around 800 rollouts in the aggregated dataset. After around 20k gradient steps, it seems to surpass the best-performing BC distillation runs using more than 10k rollouts and 500k gradient steps, at which point it has $\sim 1.5k$ demonstrations in the replay buffer. This result highlights the effectiveness of online and interactive learning as opposed to learning purely passively from an offline dataset. Furthermore, it highlights that the expert we query is an effective teacher. It also highlights that for interactive learning to be effective, one needs to have a teacher ready to be queried as learning progresses.

APPENDIX IX

RESIDUAL RL ABLATIONS

A. Effect of fully versus partially closed-loop policies

One differentiating factor of our residual model from some prior work is that the base and residual models make predictions at different frequencies, i.e., every 8 timesteps for the base model and every timestep for the residual model. Making predictions with the most up-to-date information is likely an easier prediction problem, and we expect this to work better than the “standard” setup of letting the residual correct the full output of the base model. When training a residual model

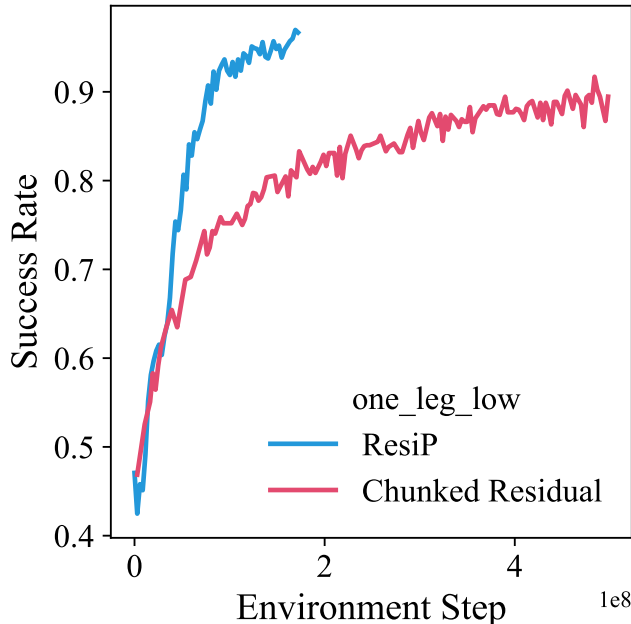


Fig. 23. When learning a residual correction term that corrects the whole chunk at a time online, we find that the learning is significantly slower (measured in environment steps) and saturates a lower asymptotic level.

that corrects a whole chunk at a time but otherwise uses the same hyperparameters, we observe that training is less sample efficient and performance saturates at a lower success rate. In particular, the chunked residual policy reaches $\sim 85\%$ success rate in about 250 million environment steps, while the one-step residual needs about 75 million.

To further probe the difference between fully closed-loop policies and those using chunking, we evaluate the policies with perturbations added to the parts in the environment throughout the episode. In particular, at each timestep, 1% of parts across the environments will have a random force applied to them. The forces are sampled from the same distribution as the initial part randomization distribution.

See Fig. 5 and Tab. XIV for results. We generally see that the partially open-loop policies have a bigger drop in performance when perturbations are introduced, around 20 percentage points compared to 12 for the one-step residual model.

Model	No Perturb	W/ Perturb	Drop in SR
Standard RPPO	98%	86%	12 pp
Chunked RPPO	92%	73%	19 pp
Chunked pre-trained BC	52%	32%	20 pp
Dagger chunked student DP	90%	68%	24 pp

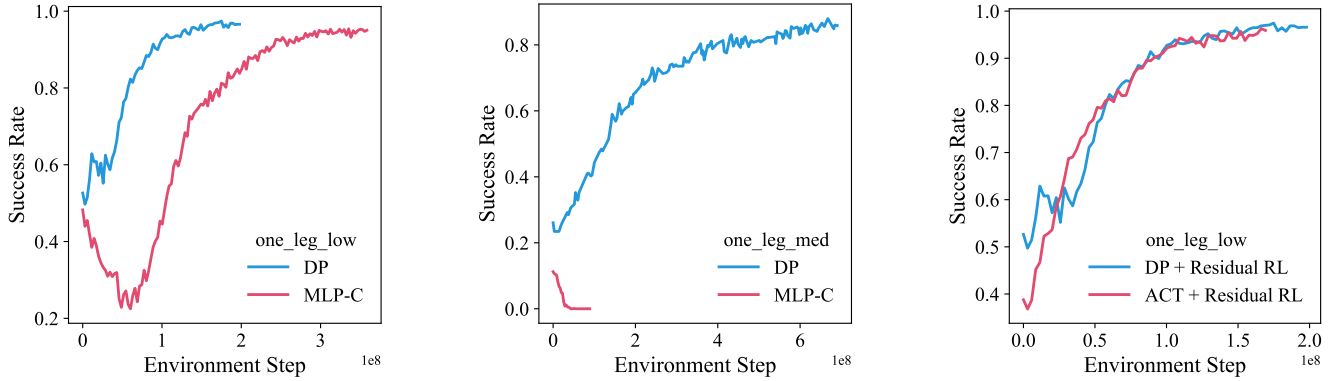
TABLE XIV. Success rates with/without perturbations for different models. SR = Success Rate, pp = percentage points.

B. Residual base policy ablation

a) MLP as base: To further tease apart what part of the diffusion policy that provides the most important performance increase, the action chunking or the denoising diffusion process, we run the same residual PPO run for the `one_leg` task as before, but with the best-performing BC MLP model in place of the diffusion policy. The results are shown in Fig. 24a and Fig. 24b. The resulting training dynamics are intriguing. Despite the initial success rate of the base model being close to that of the diffusion model, the success rate drops markedly when exploration noise is introduced. This is especially visible in the training performance in plot 2 below. We also notice that the evaluation performance drops as the residual model explores and learns more. However, the residual is eventually able to find actions that the MLP responds better to and, in the end, converges to a similar performance as the diffusion-based runs. In the more challenging task with higher initial state randomness, the same initial dynamic plays out, but the training performance drops to zero, causing the learning to collapse. We conclude that any base model achieving a high enough initial success rate can be plugged into our framework (and, based on our BC experiments, a base model with chunking is likely to outperform one without chunking) but that the expressivity and robustness to input noise offered by diffusion de-noising also contributes to downstream performance

benefits during residual RL.

b) ACT as base: To see if the robustness to noise and suitedness for residual learning is unique to the diffusion-type model, we also implement and test using Action-Chunked Transformer (ACT) [6] as the base model for the `one_leg` task at low randomness. We find that, with some tuning, the ACT model can achieve comparable performance as the diffusion model, though slightly lower, in pre-training. In the fine-tuning phase, however, it functions as well and stably as the diffusion model base, as shown in Fig. 24c. This points toward the residual RL framework being suitable for a wide range of fine-tuning applications and may be applied in fine-tuning even larger and possibly multi-task models.



(a) Evaluation success rates for RL training for `one_leg`, low randomness for Diffusion and MLP base policy.

(b) Evaluation success rates for RL training for `one_leg`, medium randomness for Diffusion and MLP base policy.

(c) Evaluation success rates for RL training for `one_leg`, low randomness for Diffusion and ACT base policy.

Fig. 24. We compare the diffusion-based residual RL training performance with the best-performing MLP as the base model in (a) and (b). As we can see, despite having similar pre-training performance (for low randomness), the MLP-based residual model performs poorly compared to the diffusion-based one. On a higher randomness setting, it fails to complete the task. We compare with using the ACT [6] as the base policy in (c). The pre-training performance is slightly worse, but performance quickly catches up during online learning, indicating that the ACT model is also well-suited for residual learning.

C. Residual action scaling parameter ablation

A design choice we make is the parameter $\alpha = 0.1$. The parameter choice is somewhat arbitrary and was informed by some intuitions about the task. For example, since the residual model intends to make local corrections, we want to imbue it with that inductive bias. In the normalized action space, the workspace is constrained to $[-1, 1]$, and letting a $\sigma = 1$ for the residual Gaussian model correspond to $[-0.1, 0.1]$ on the macro scale seemed reasonable.

We have tested more values of the parameter $\alpha \in \{0.01, 0.05, 0.2, 1.0\}$, but kept the resulting exploration noise on the macro scale fixed (i.e., scaled with the value of α , so $\alpha_1\sigma_1 = \alpha_2\sigma_2$). The result, shown in the figure below, shows a remarkable robustness to this parameter, and all cases have very similar performance.

We note a couple of observations. First, $\alpha = 0.2$ seems to perform slightly better than our original $\alpha = 0.1$. Second, different levels of α also result in very different magnitudes of activations at the last layer, which impacts losses. This experiment shows that the resulting performance does not differ significantly, but we suspect it could make training less stable in harder settings.

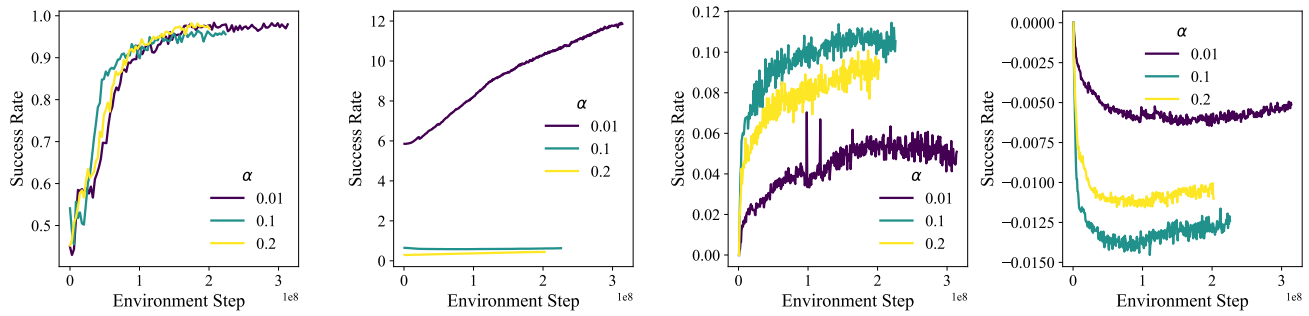


Fig. 25. We test different values of the residual action scaling parameter α and test it for values $\alpha \in \{0.01, 0.1, 0.2\}$ while adjusting the exploration noise to be such that the macro-level exploration is the same initially. We find that for success rates in this task, the value is not crucial but does cause training dynamics to change, particularly the residual model output norms and policy loss magnitude.